



AOP

ARMAGH  
OBSERVATORY &  
PLANETARIUM



# PHYSICAL AND DYNAMICAL PROPERTIES OF SELECTED EARTH CO-ORBITAL ASTEROIDS



GALIN B. BORISOV<sup>1,2</sup>,

APOSTOLOS A. CHRISTOU<sup>2</sup>, GORDANA APOSTOLOVSKA<sup>3</sup>

1. INSTITUTE OF ASTRONOMY WITH NAO, BULGARIAN ACADEMY OF SCIENCES

2. ARMAGH OBSERVATORY AND PLANETARIUM, UK

3. INSTITUTE OF PHYSICS, FACULTY OF NATURAL SCIENCES AND MATHEMATICS,  
UNIVERSITY OF SKOPJE, MACEDONIA

# INTRODUCTION

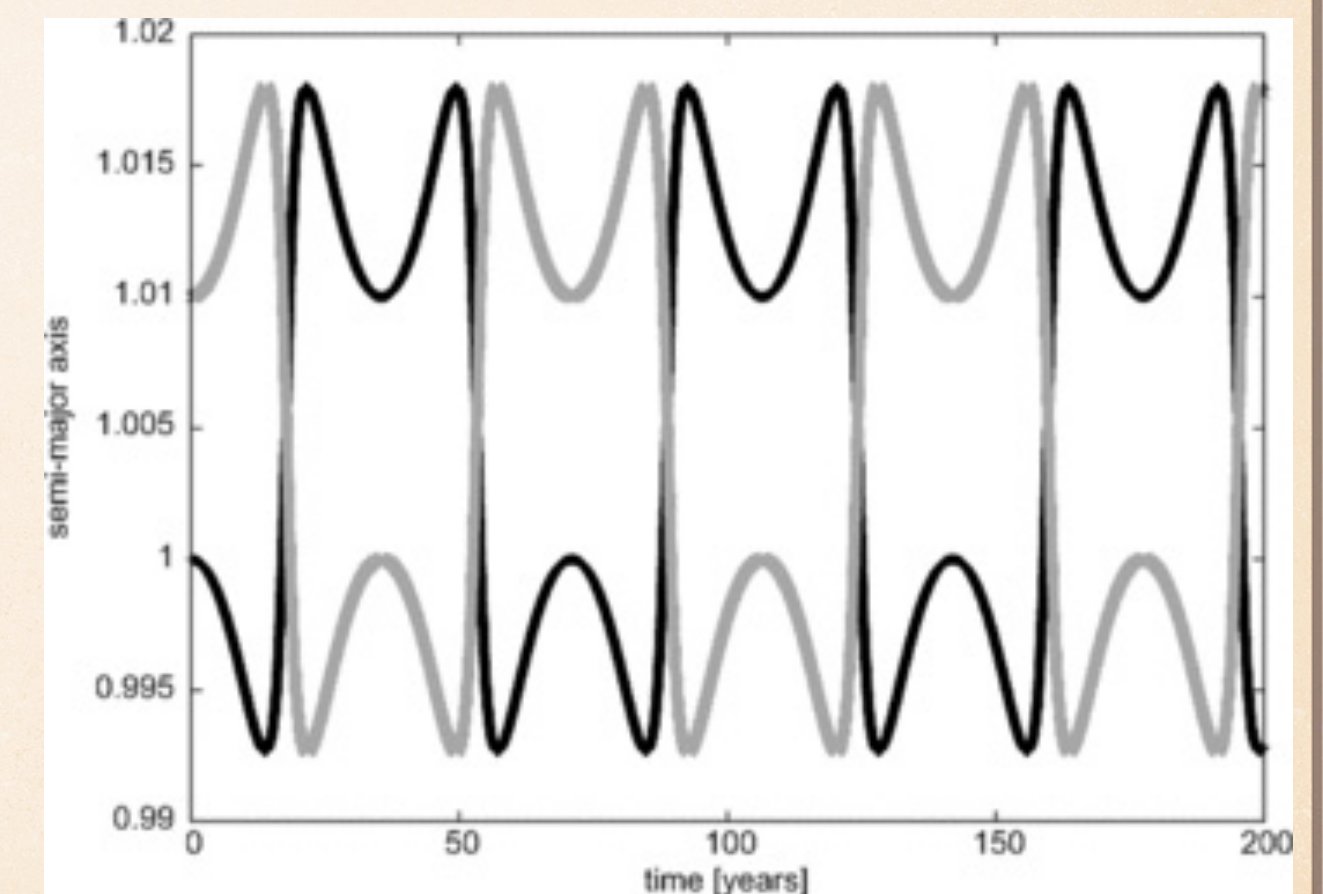
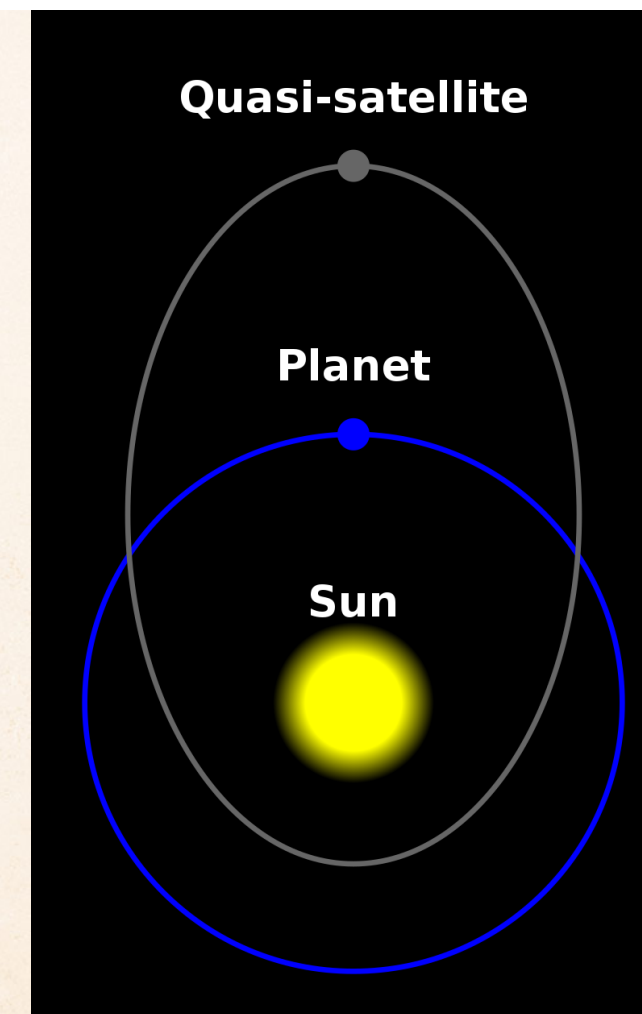
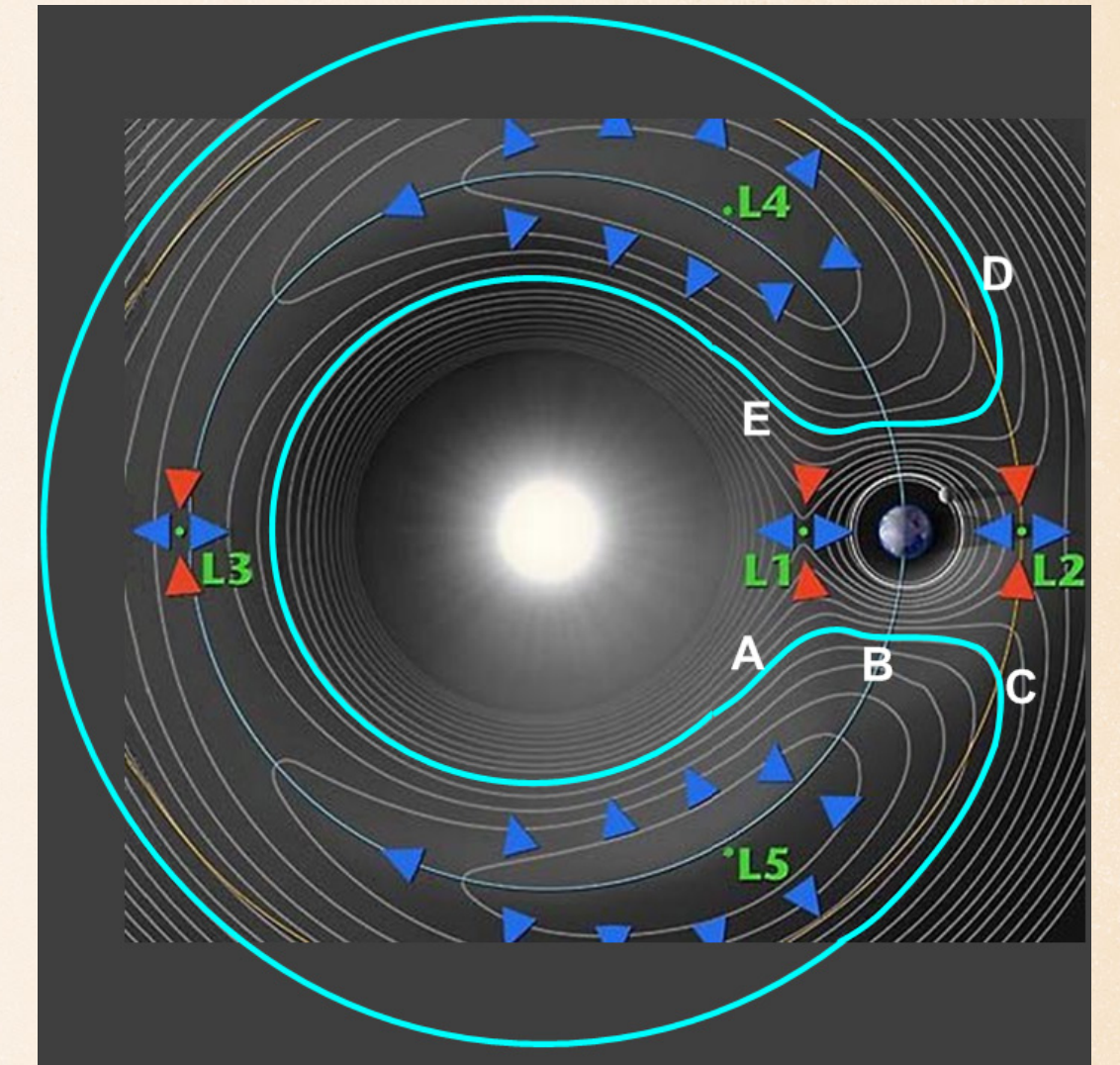
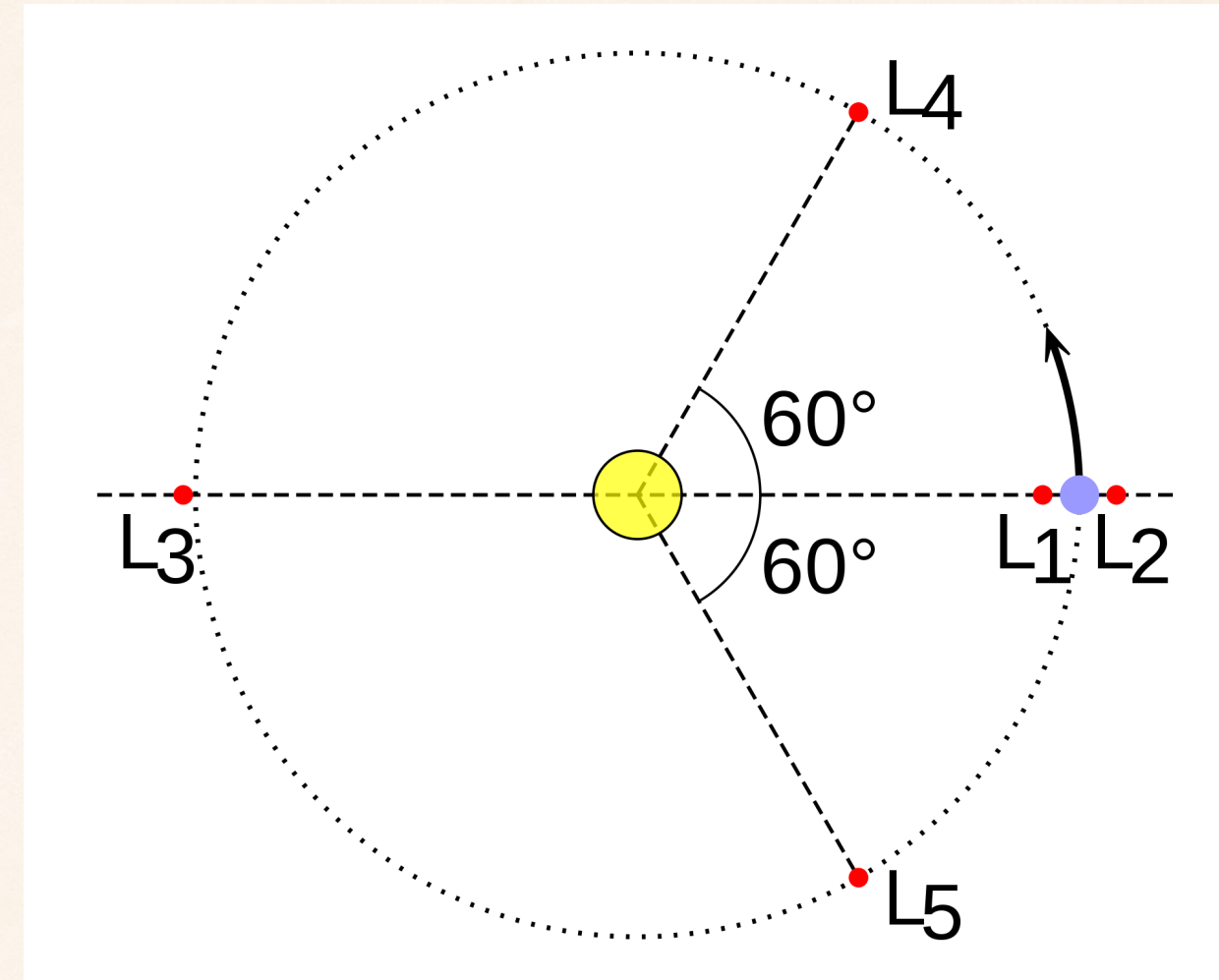
- ◆ Earth co-orbital asteroids - Asteroids with an average heliocentric distance of 1 AU.
- ◆ They present a special challenge to Earth-based surveys.
- ◆ This leads to a much lower observational completeness for these types of objects.
- ◆ Co-orbital asteroids are generally thought to have more stable orbits.

# CO-ORBITAL CONFIGURATION

- ❖ In astronomy, a co-orbital configuration is a configuration of two or more astronomical objects (such as asteroids, moons, or planets) orbiting at the same, or very similar, distance from their primary, i.e. they are in a 1:1 mean-motion resonance. (or 1:-1 if orbiting in opposite directions).

# CO-ORBITAL CONFIGURATION

- ❖ Trojans - objects orbit  $60^\circ$  ahead of ( $L_4$ ) or behind ( $L_5$ ) a more massive object
- ❖ Horseshoe orbits - Objects librating around  $180^\circ$  from the primary. Their orbits encompass both equilateral Lagrangian points, i.e.  $L_4$  and  $L_5$
- ❖ Quasi-satellite - co-orbital objects that librate around  $0^\circ$  from the primary.
- ❖ Exchange orbits



# PHOTOMETRIC OBSERVATIONS - DENSE DATA

- ❖ Photometric observations of selected Earth co-orbital asteroids were carried out from the Bulgarian National Astronomical Observatory - Rozhen, using the Two-channel Focal Reducer Rozhen or “FoReRo2” instrument attached to the 2-m RCC telescope



Number	Designation	yyyy mm dd	Phase	L <sub>PAB</sub>	B <sub>PAB</sub>	Grp
(418849)	2008 WM64	2017 12 25	36.9	96	19	APO
(138175)	2000 EE104	2018 11 09	66.0	100	8	APO
—    —	—    —	2019 01 01	19.3	108	14	APO
—    —	—    —	2020 01 02	17.9	104	14	APO
	2017 SL16	2020 09 22	30.0	14	6	ATE
	2016 CA138	2020 02 17 & 18	20.3	158	-7	ATE

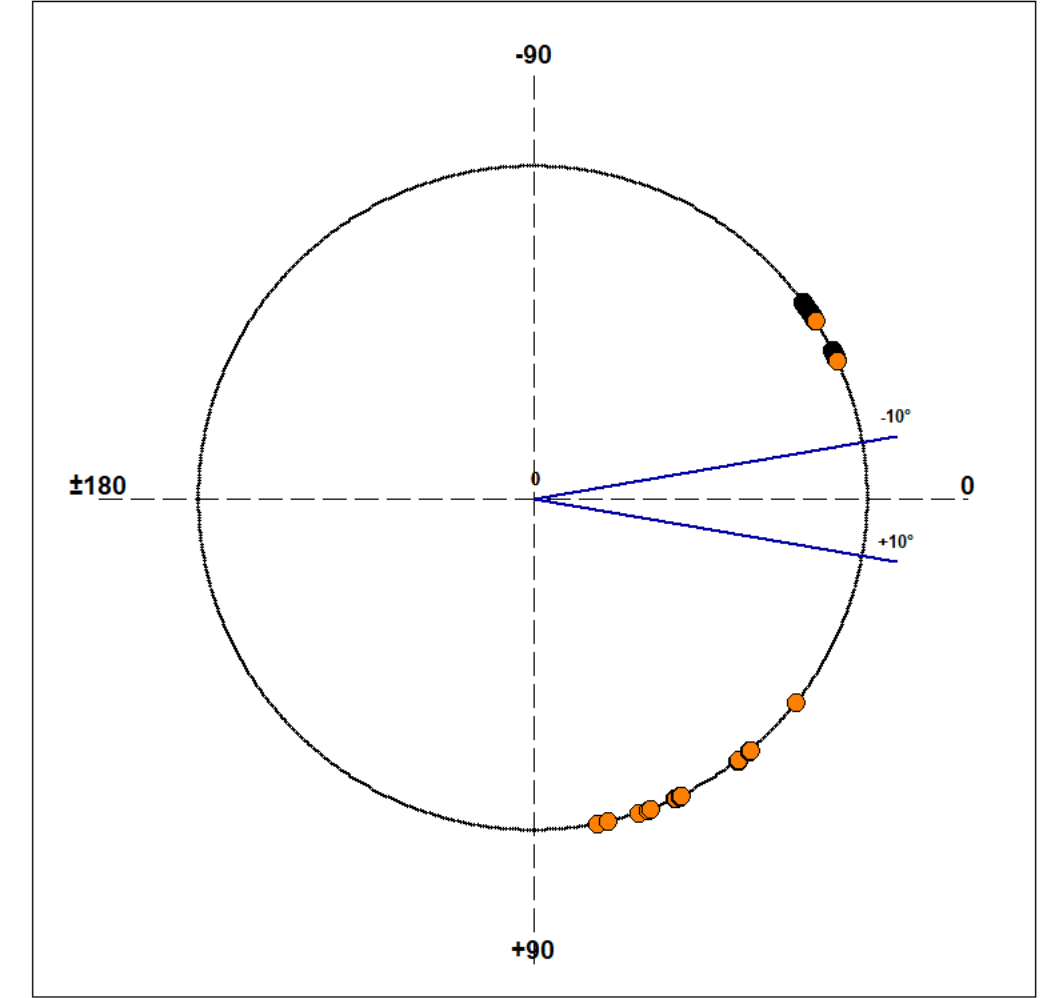
# PHOTOMETRIC OBSERVATIONS - SPARSE DATA

- ❖ In addition, we are considering available sparse data on the asteroids taken from the AstDys-2 database, choosing to use only those measurements with an reported accuracy of 0.01 magnitude or higher

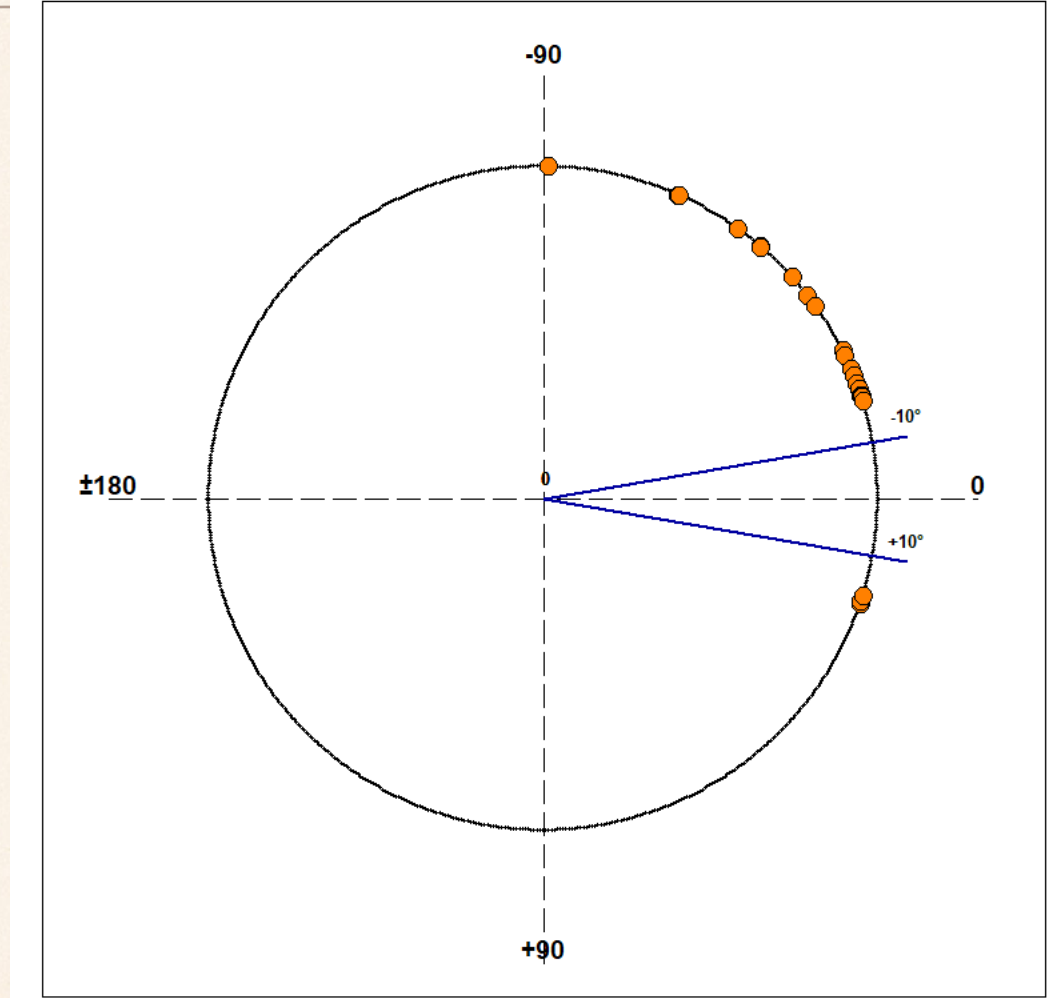
Number	Designation	yyyy mm dd	Filter	Obs. Code <sup>a</sup>
(418849)	2008 WM64	2019 01 07	c	T08 <sup>b</sup>
		2019 01 09	c	T05 <sup>c</sup>
		2018 12 19	o	T08
		2018 12 21	o	T05
		2018 12 24	o	T08
		2018 12 28	o	T05
		2020 01 02	o	T08
		2020 12 20	o	T08
		2020 12 22	o	T05
		2020 12 29	o	T08
		2021 01 03	o	T08
(138175)	2000 EE104	2019 01 09	c	T05
		2019 12 27	c	T05
		2020 12/11	c	T08
		2018 12 28	o	T05
		2019 12 08	o	T08
		2020 01 02	o	T08
		2020 12 09	o	T05
		2020 10 19	G	G96 <sup>d</sup>
		2020 11 12	G	703 <sup>e</sup>
		2020 11 24	G	703
		2020 11 29	G	G96
		2020 12 19	G	G96
		2020 12 20	G	703
		2020 12 26	G	703
		2021 01 03	G	G96
2021 01 05	G	703		
	2017 SL16	2020 09 23	G	I52 <sup>f</sup>
	2016 CA138	2019 02 15	o	T08
		2020 02 16	g	I41 <sup>g</sup>
		2020 02 16	R	I41

# ORBITAL DISTRIBUTION THE OBSERVATIONS

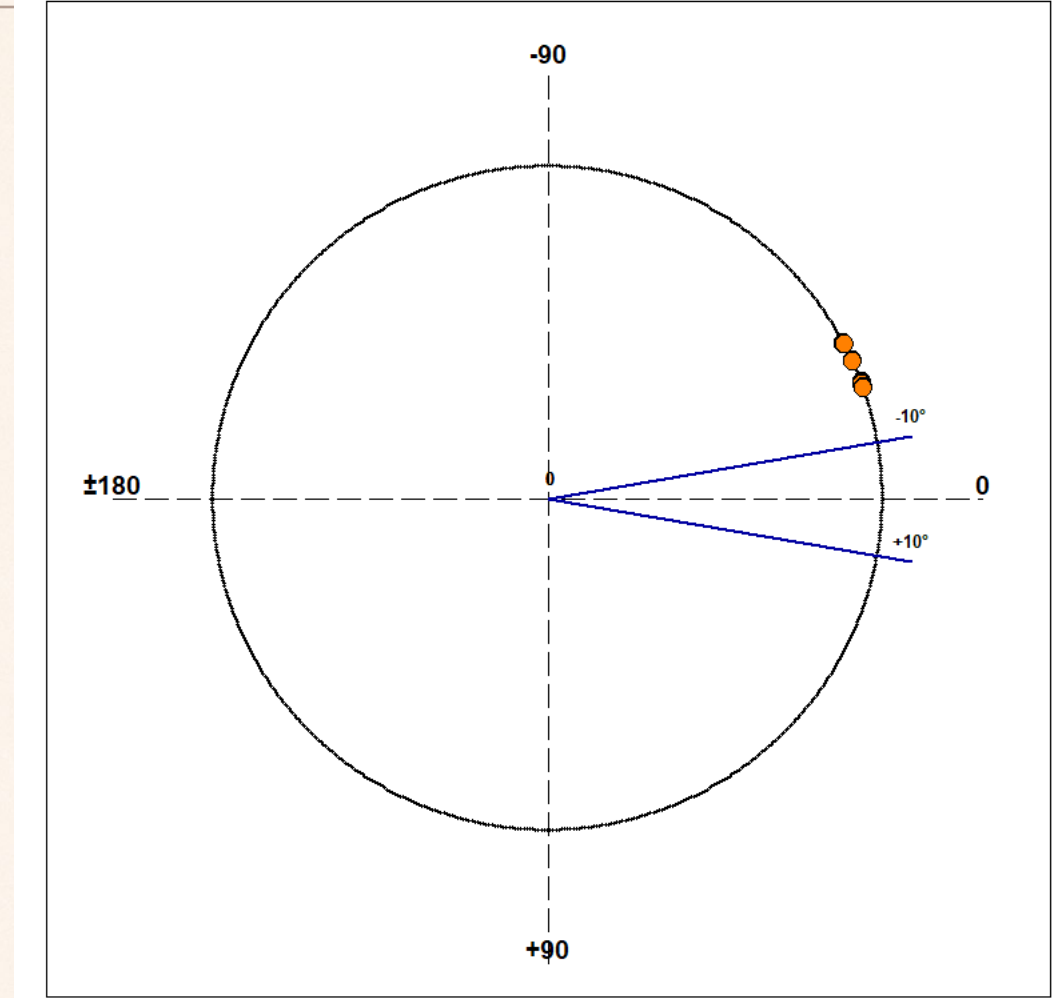
418849 2008 WM64  
Phase Angle Distribution: Minus: pre-opp Plus: post-opp



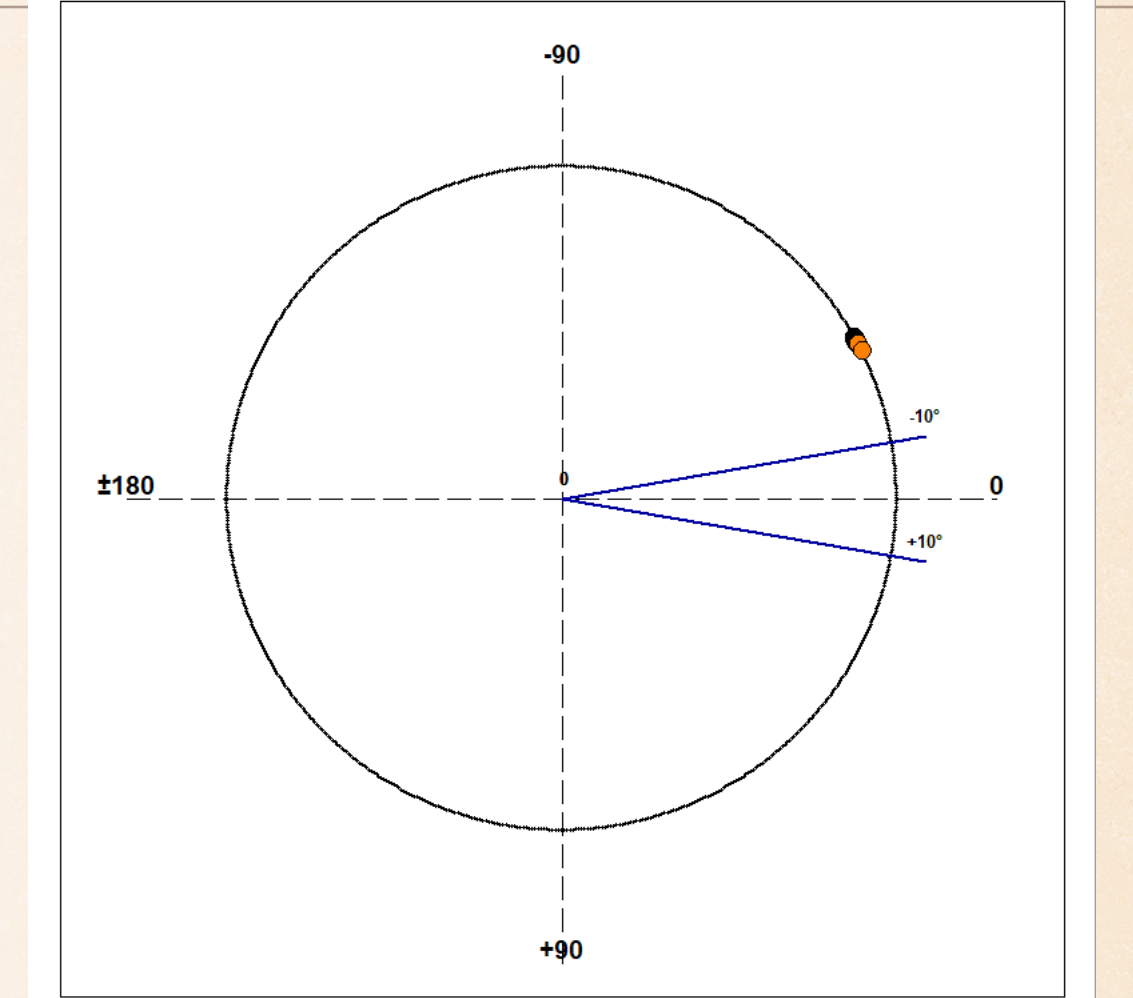
138175 2000 EE104  
Phase Angle Distribution: Minus: pre-opp Plus: post-opp



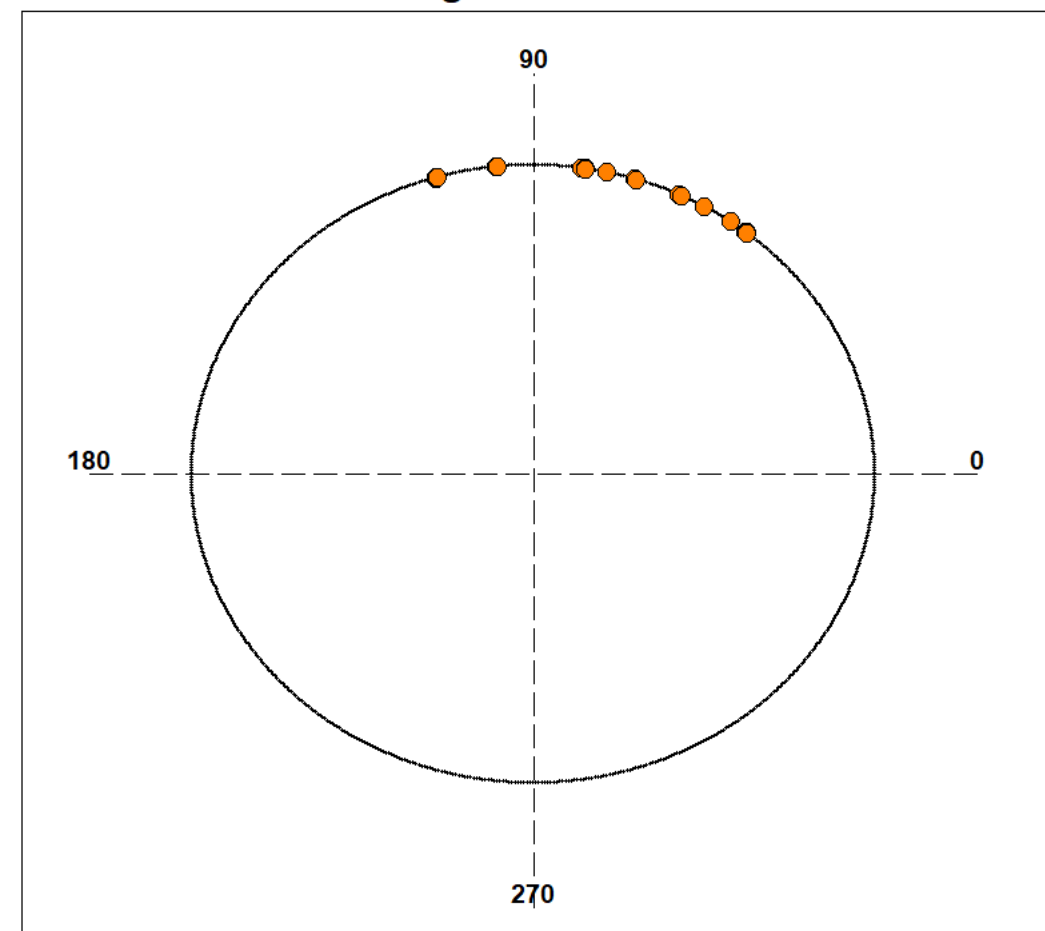
2016 CA138  
Phase Angle Distribution: Minus: pre-opp Plus: post-opp



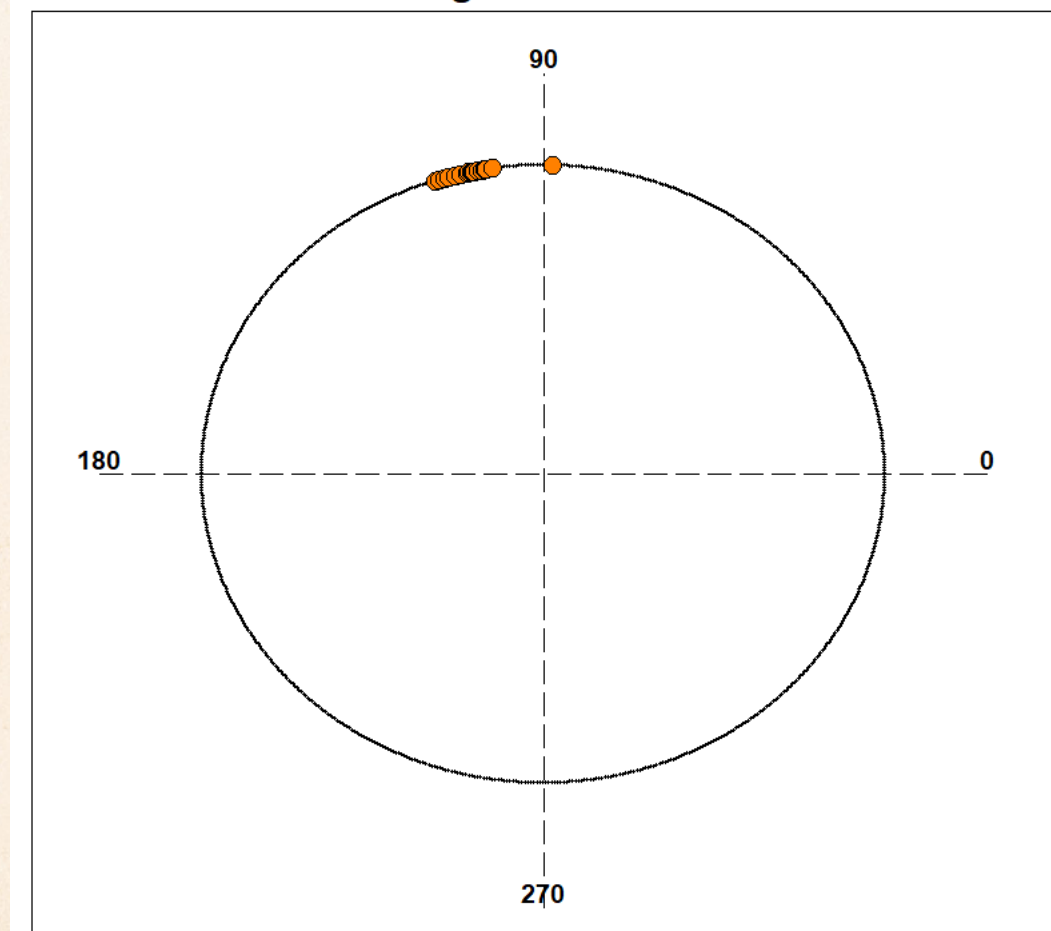
2017 SL16  
Phase Angle Distribution: Minus: pre-opp Plus: post-opp



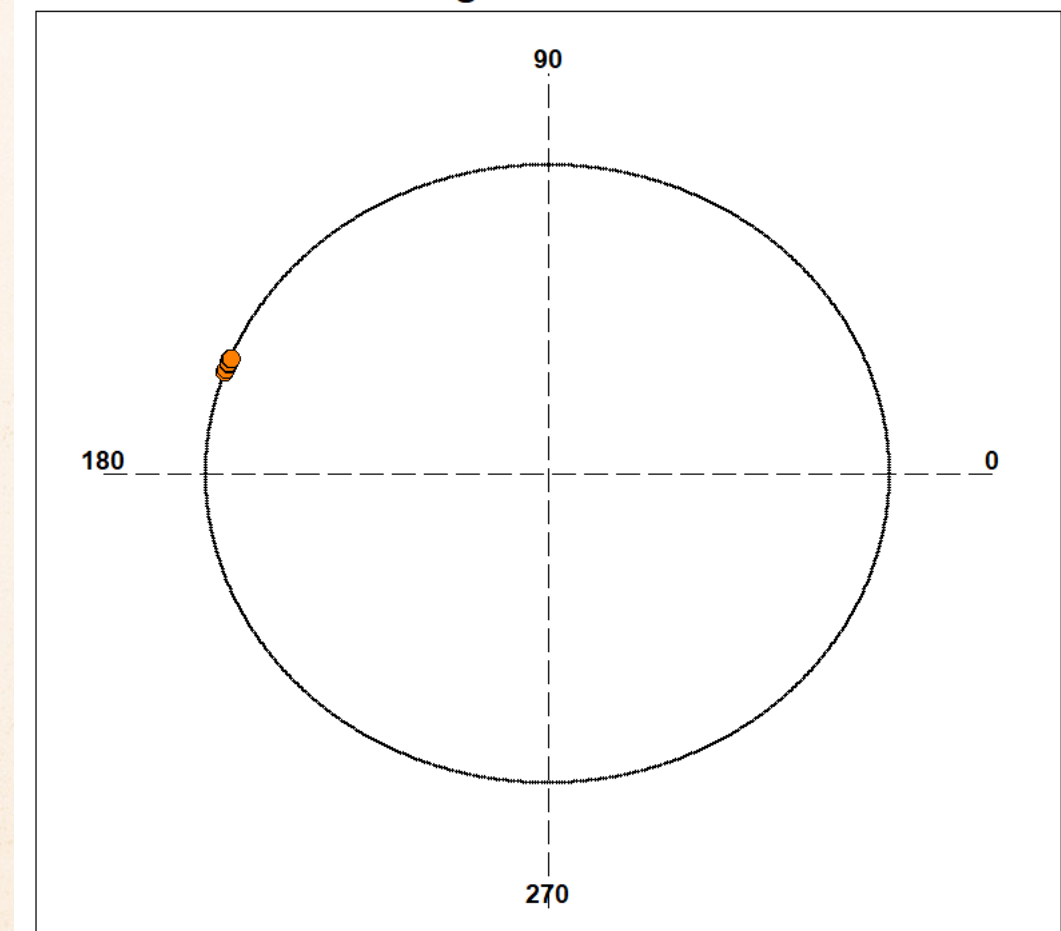
PAB Longitude Distribution



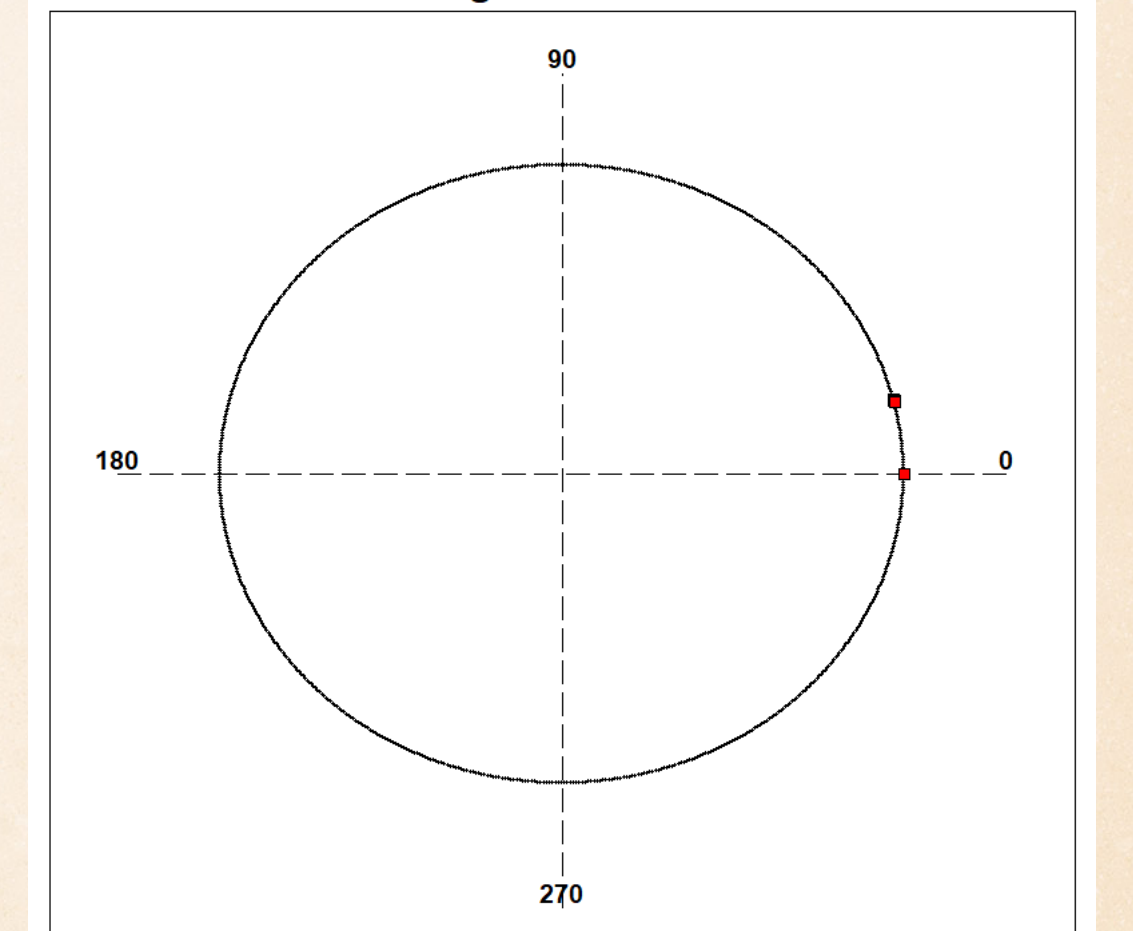
PAB Longitude Distribution



PAB Longitude Distribution



PAB Longitude Distribution



# ROTATIONAL PERIOD DETERMINATION

- ❖ Standard Fourier analysis or investigating the  $\chi^2$  of the fitted observational data by a Fourier function with different orders

We used the Fourier inversion method to determine a simple 3D shape model that reproduces the observed light curve and then we compared the curve to the observational data to obtain the best period.



# ROTATIONAL PERIOD DETERMINATION

- ❖ ~~Standard Fourier analysis or investigating the  $\chi^2$  of the fitted observational data by a Fourier function with different orders~~
- ❖ We used a light curve inversion method to determine a simple 3D shape model of the object that reproduces the modelled light curve and then we compare this light curve to the observational data to obtain the best period solution.

# ROTATIONAL PERIOD DETERMINATION

- ❖ For our purposes, we used the software provided by the Database of Asteroid Models from Inversion Techniques (DAMIT) which was developed by Mikko Kaasalainen in Fortran and converted to C by Josef Durech.
- ❖ To ensure that the global minimum of  $\chi^2$  in the period search is not missed, we scan through a fairly wide interval of possible periods.

# ROTATIONAL PERIOD DETERMINATION

- ◆ According to Kaasalainen, the smallest separation  $\Delta P$  of the local minima in the trial period  $P$  spectrum of the  $\chi^2$  of the light curve fit is roughly given by

$$\frac{\Delta P}{P} \approx \frac{1}{2} \frac{P}{T}$$

where  $T = \max(|t - t_0|)$

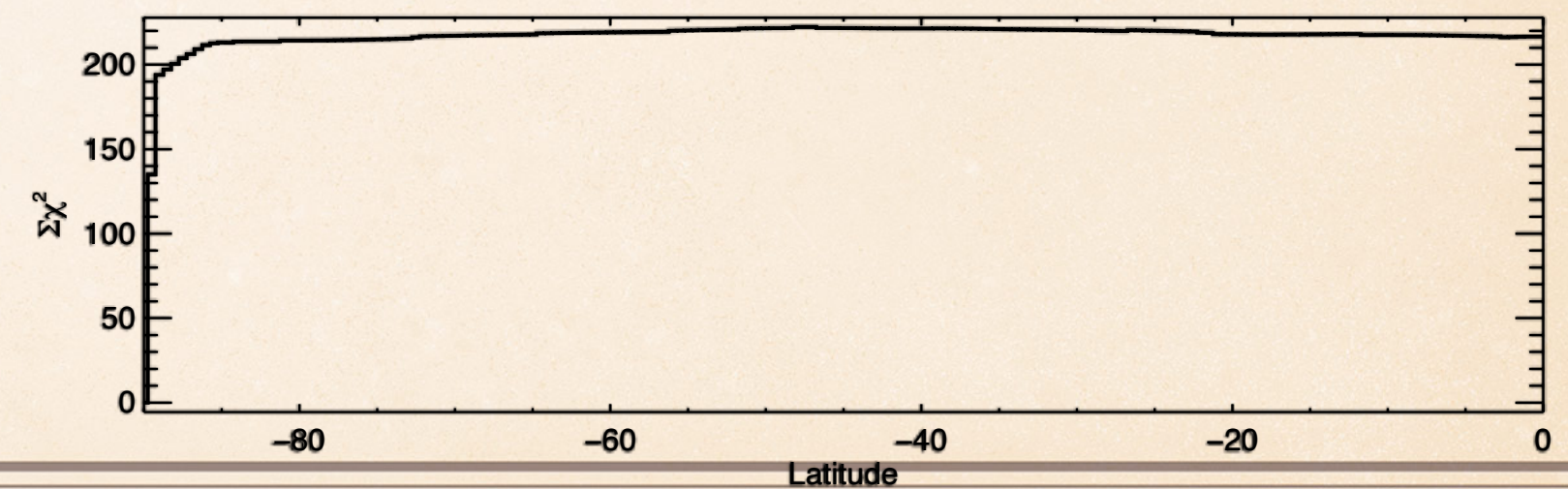
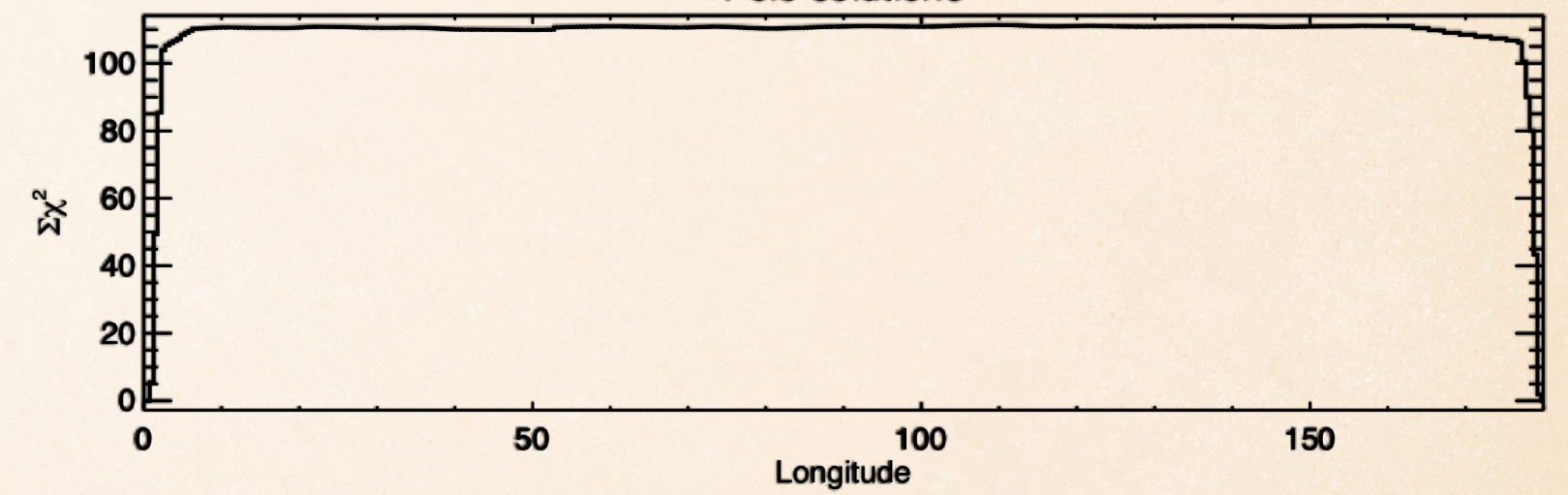
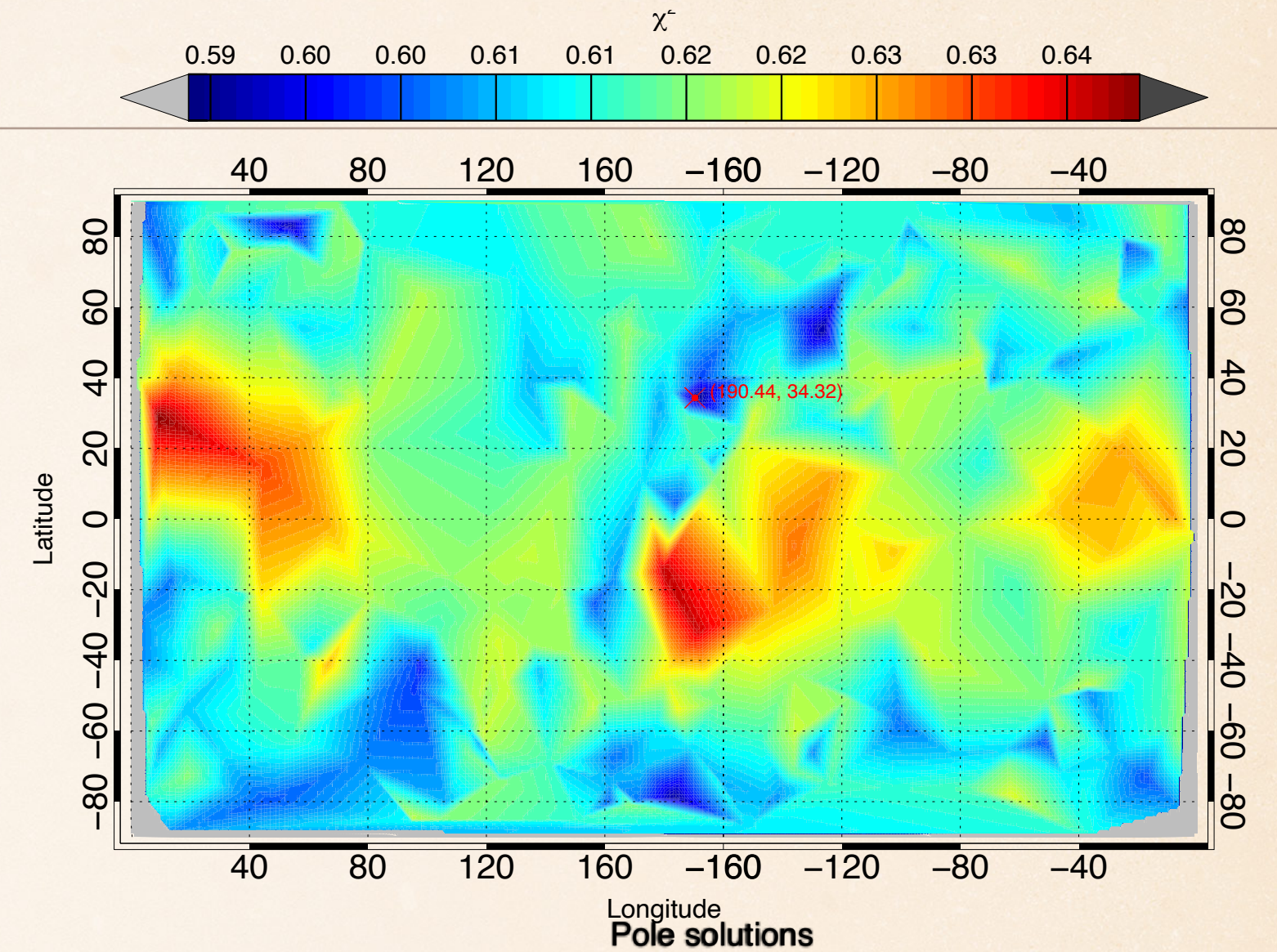
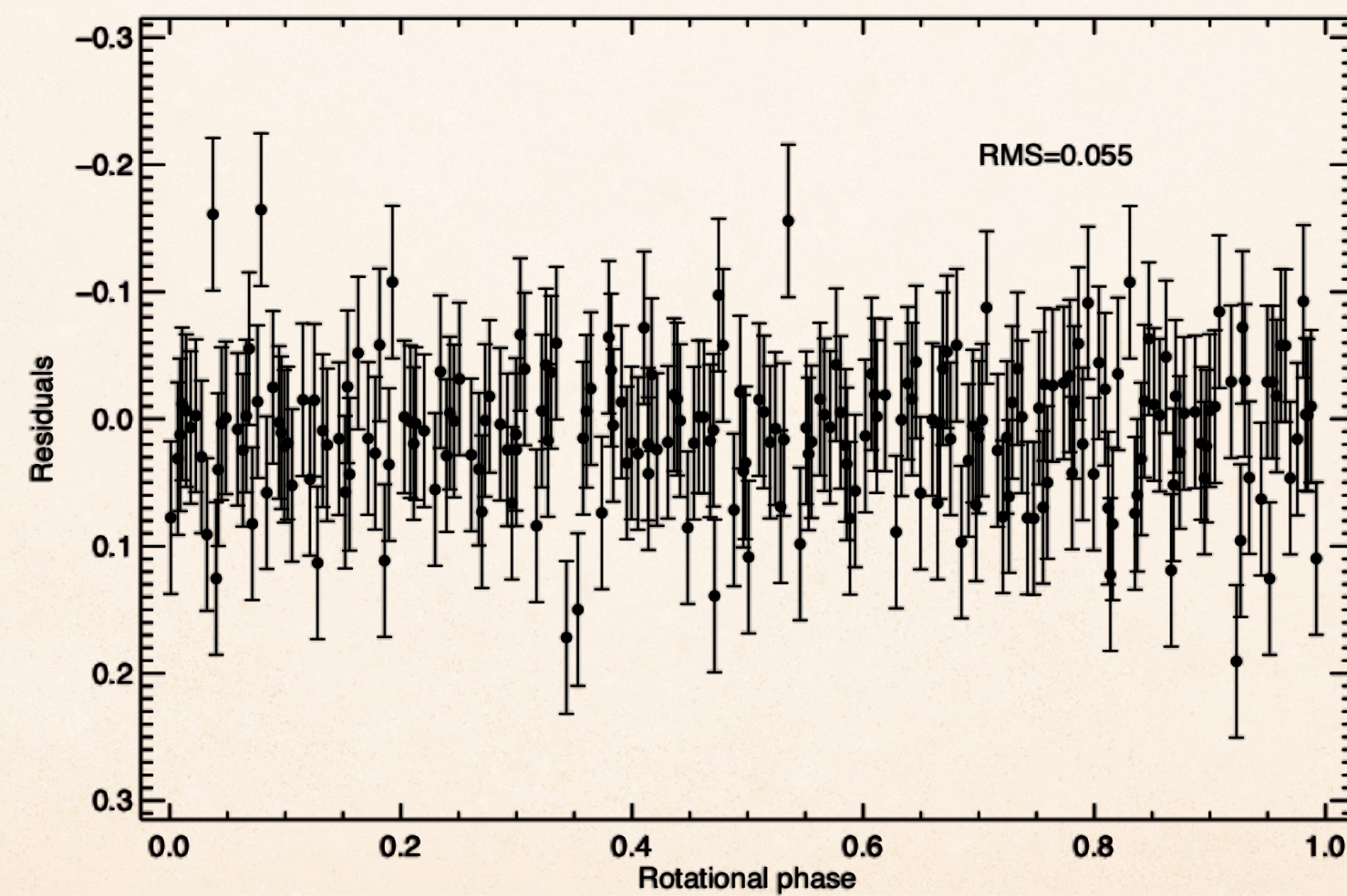
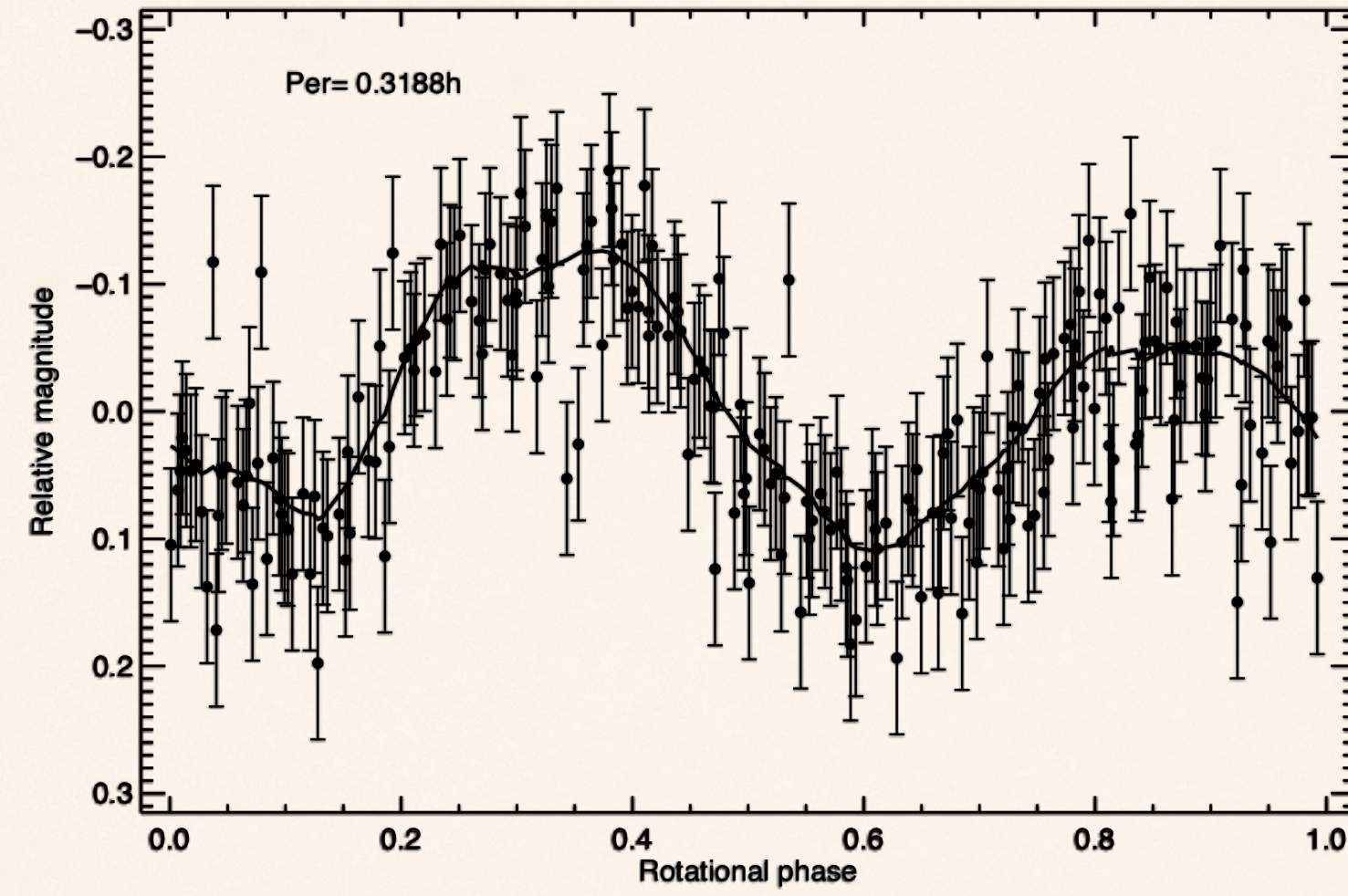
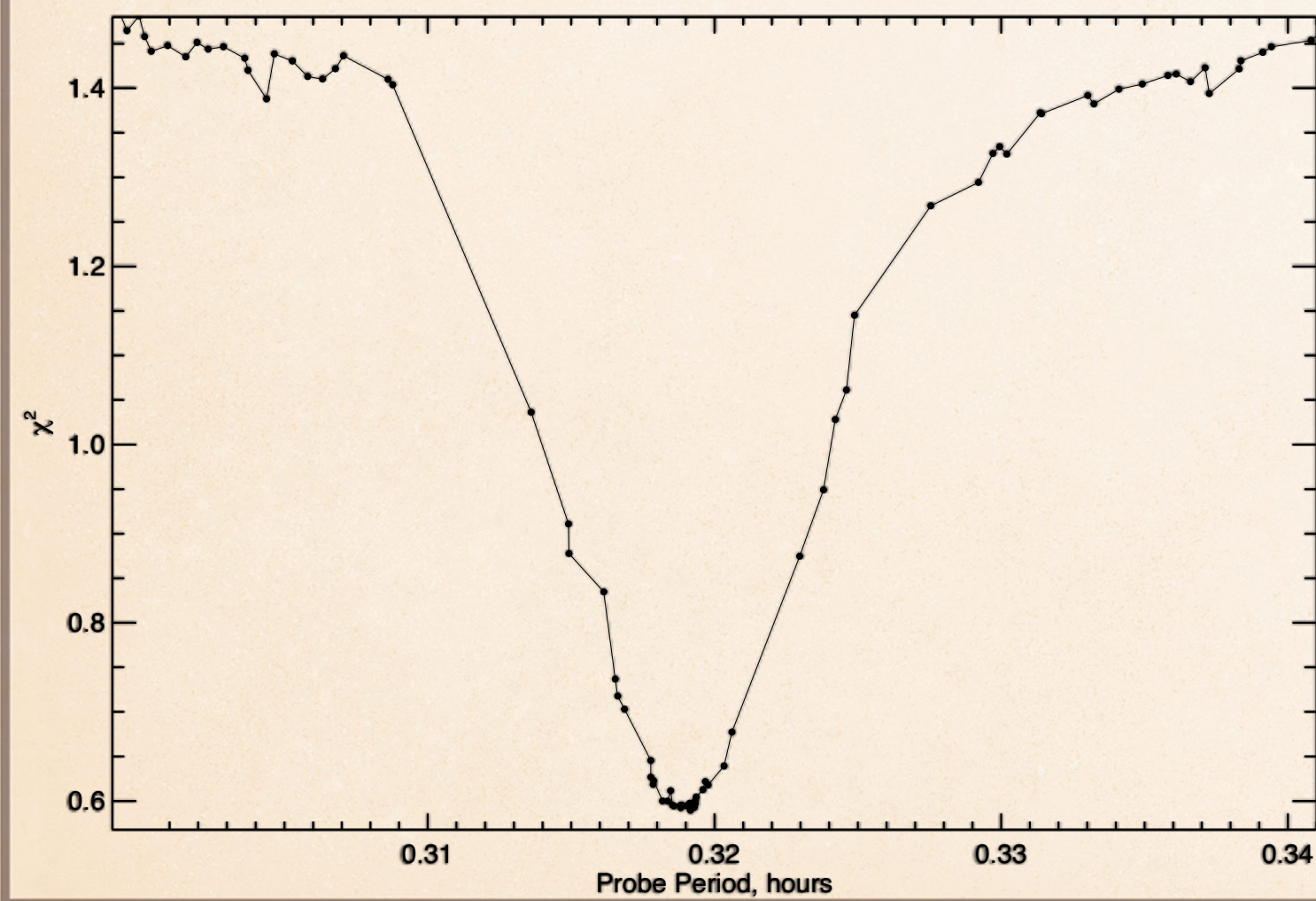
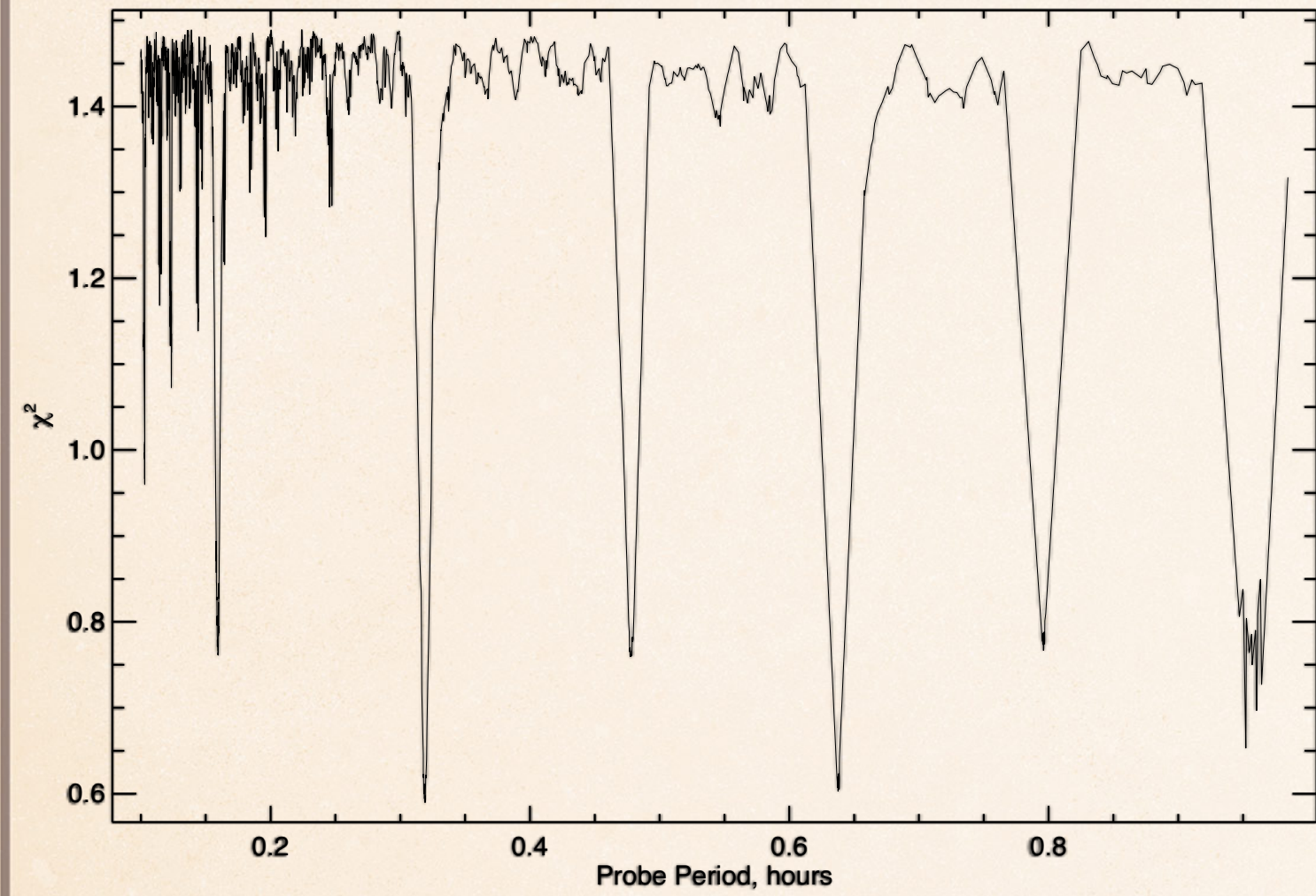
# ROTATIONAL PERIOD DETERMINATION

- ❖ Kaasalainen also explain that the period uncertainty is a hundredth part of the  $\Delta P$  for the smallest local  $\chi^2$  minimum if it is clearly lower than the others.
- ❖ But if the neighbouring minima are not clearly higher than the best one, the accuracy cannot be considered better than  $\Delta P$  since the local error estimate cannot be applied globally.

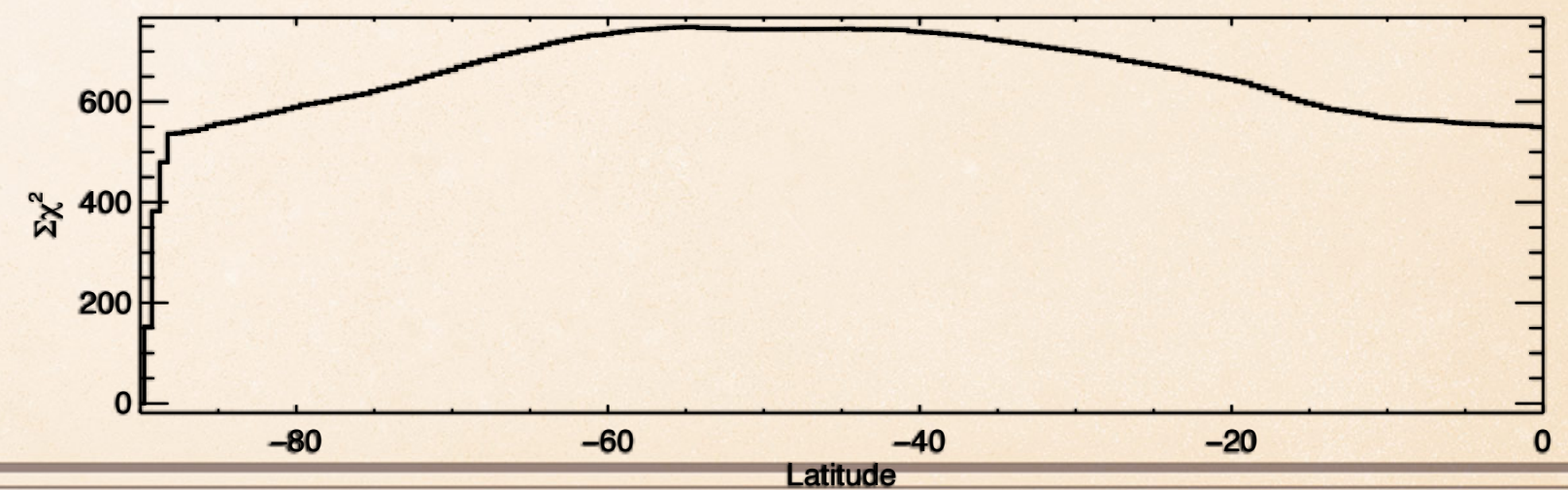
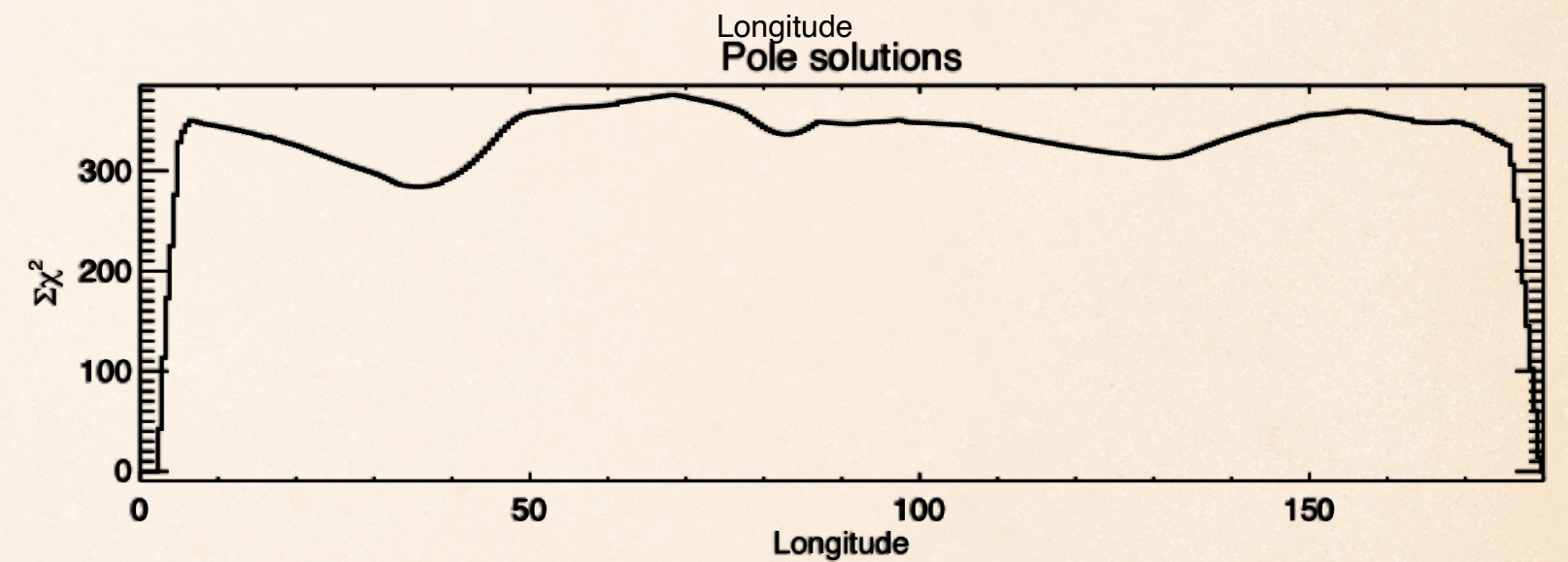
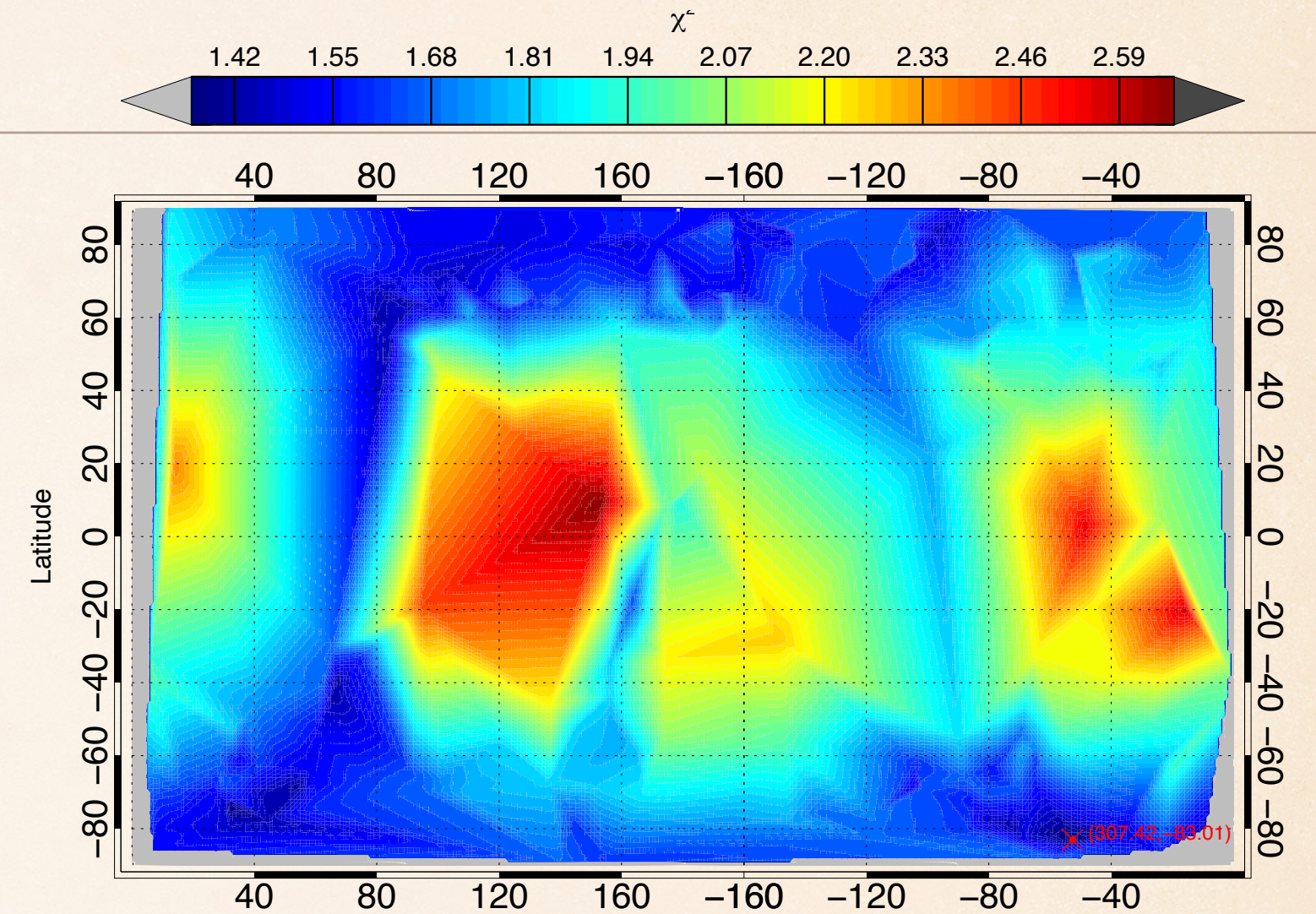
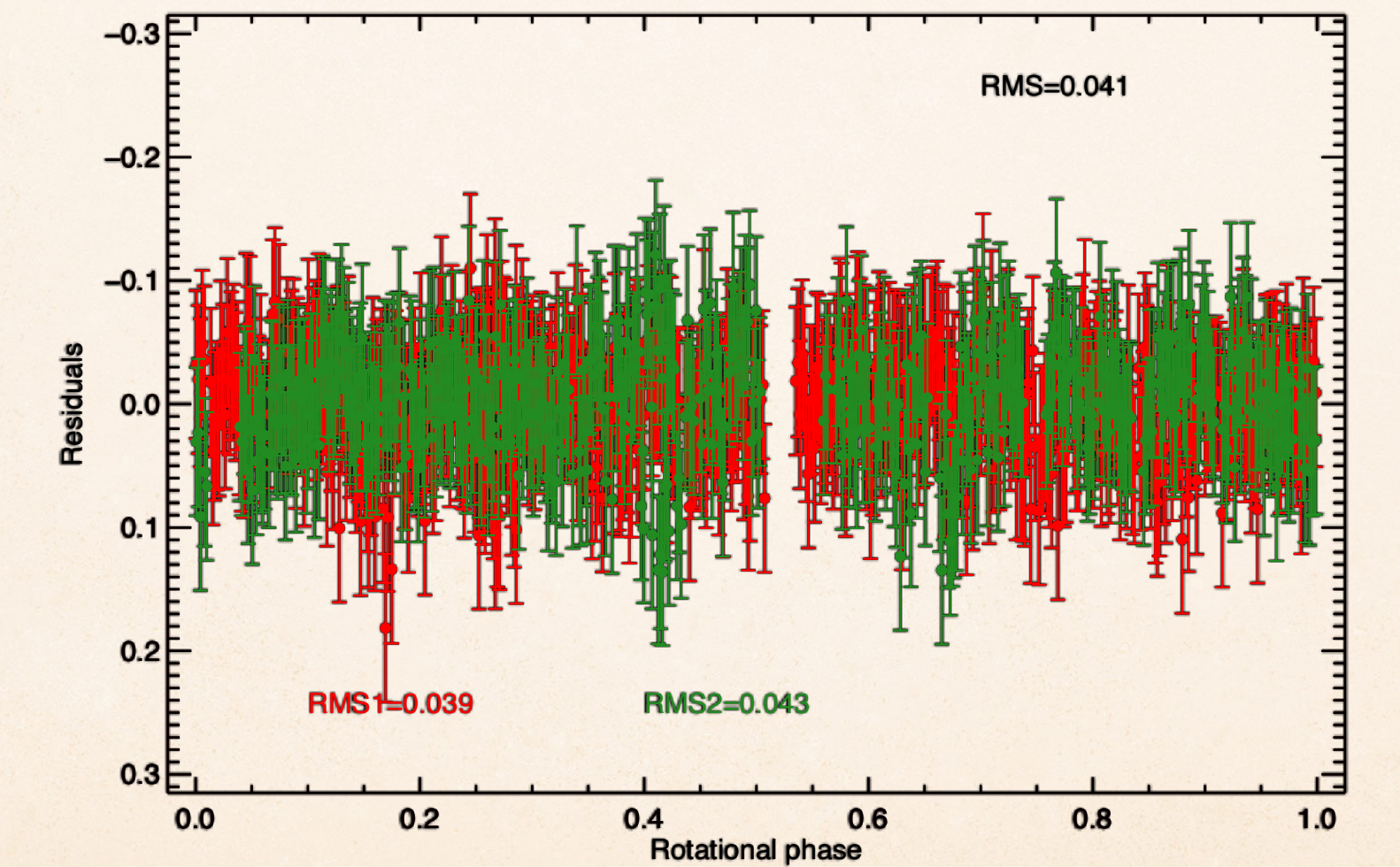
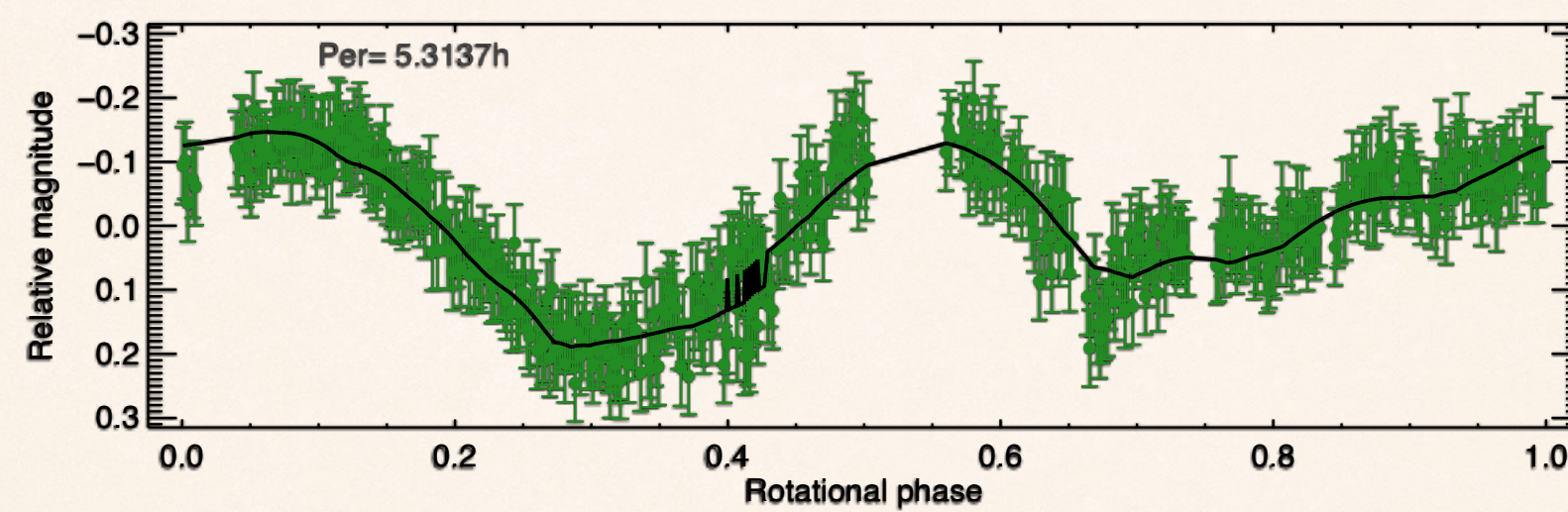
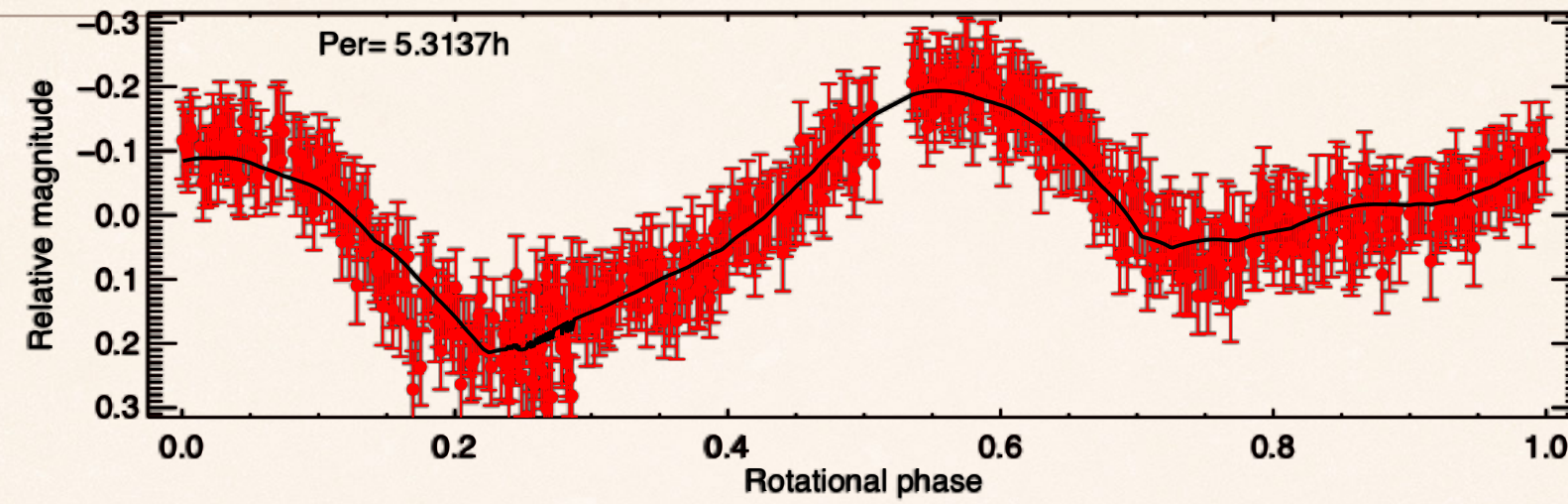
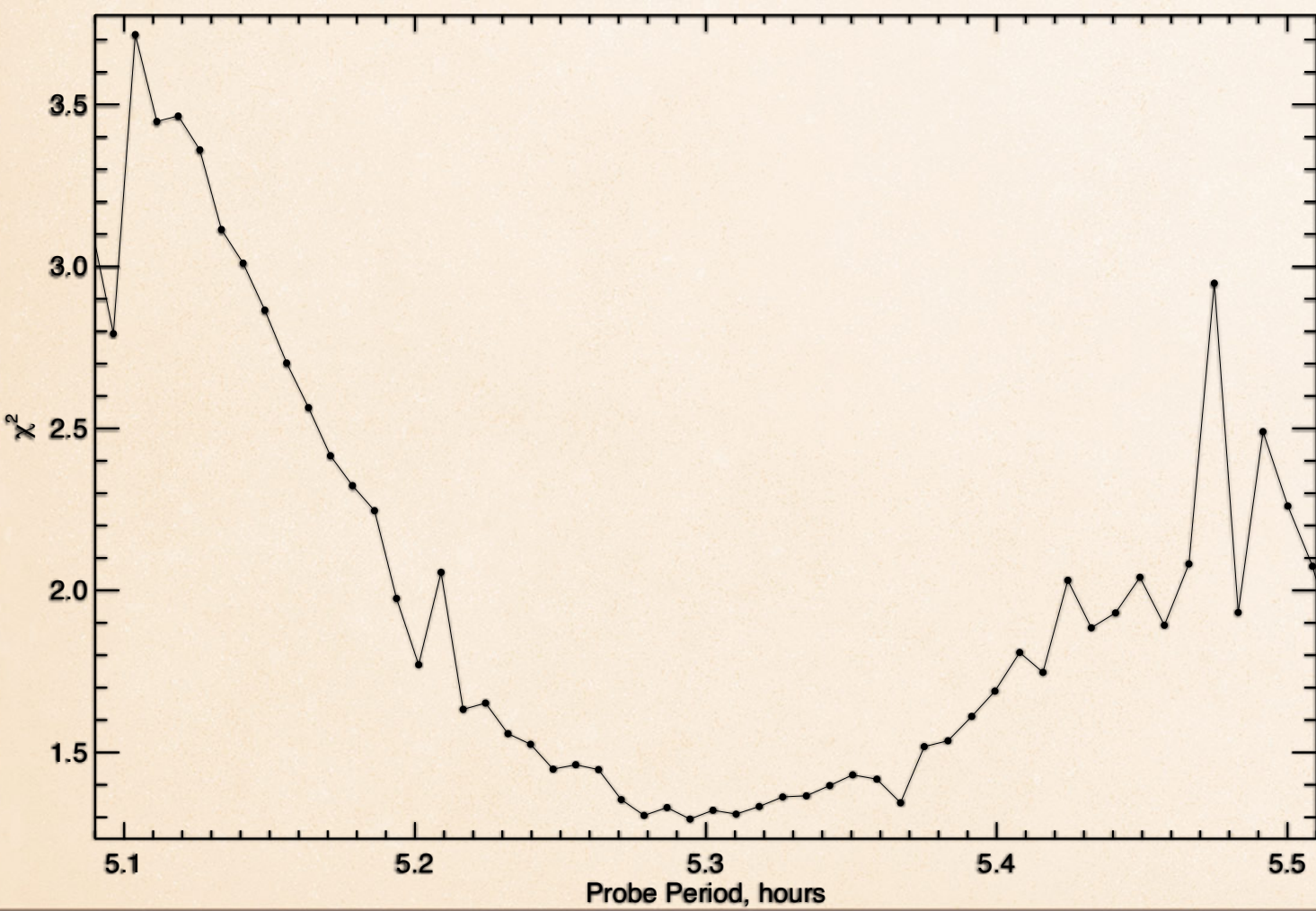
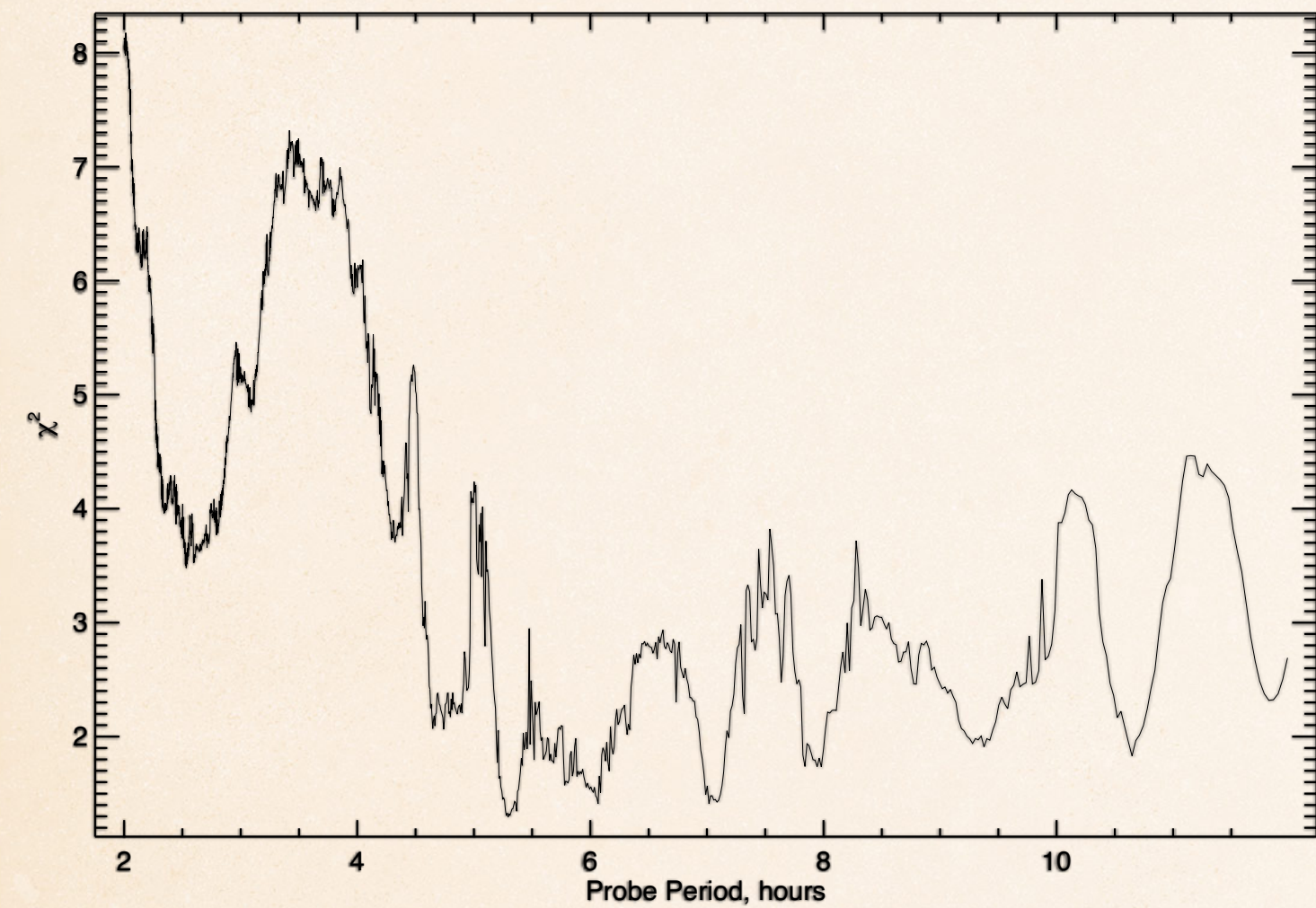
# SPIN AXIS ORIENTATION

- ❖ In order to determine a rotational pole solution for the asteroids, we ran the DAMIT `convexinv` routine with different initial poles randomly distributed over the unit sphere and with 15 deg steps in both ecliptic longitude ( $\lambda$ ) and latitude ( $\beta$ ) to produce 312 initial pole orientations which we use to contract the  $\chi^2$  maps.

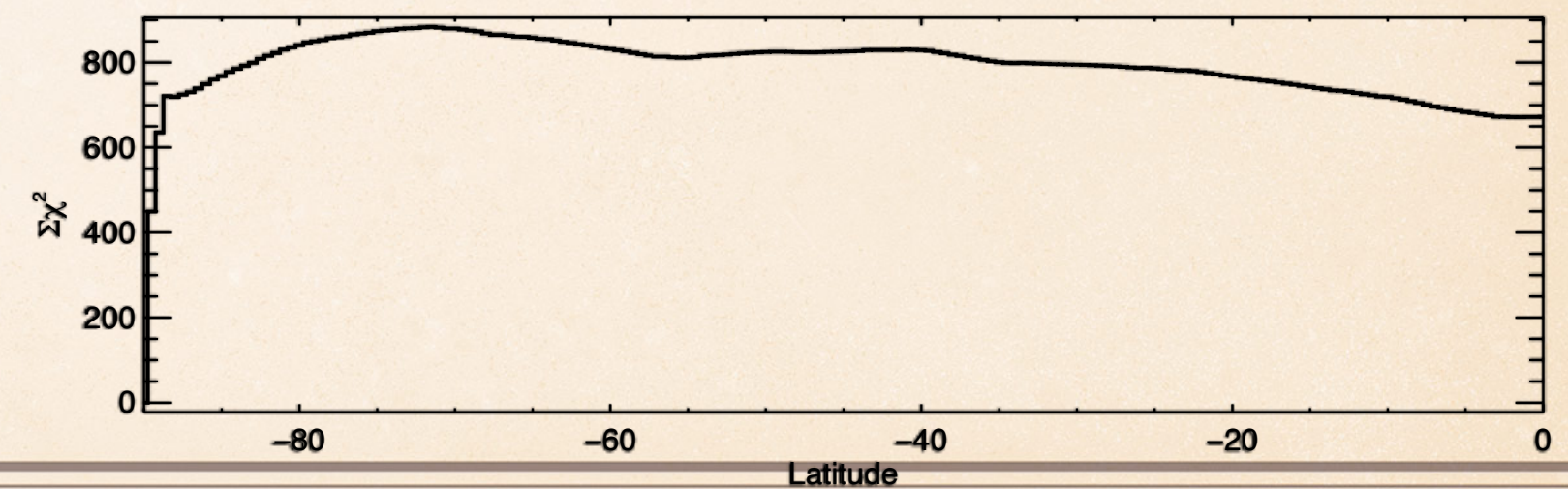
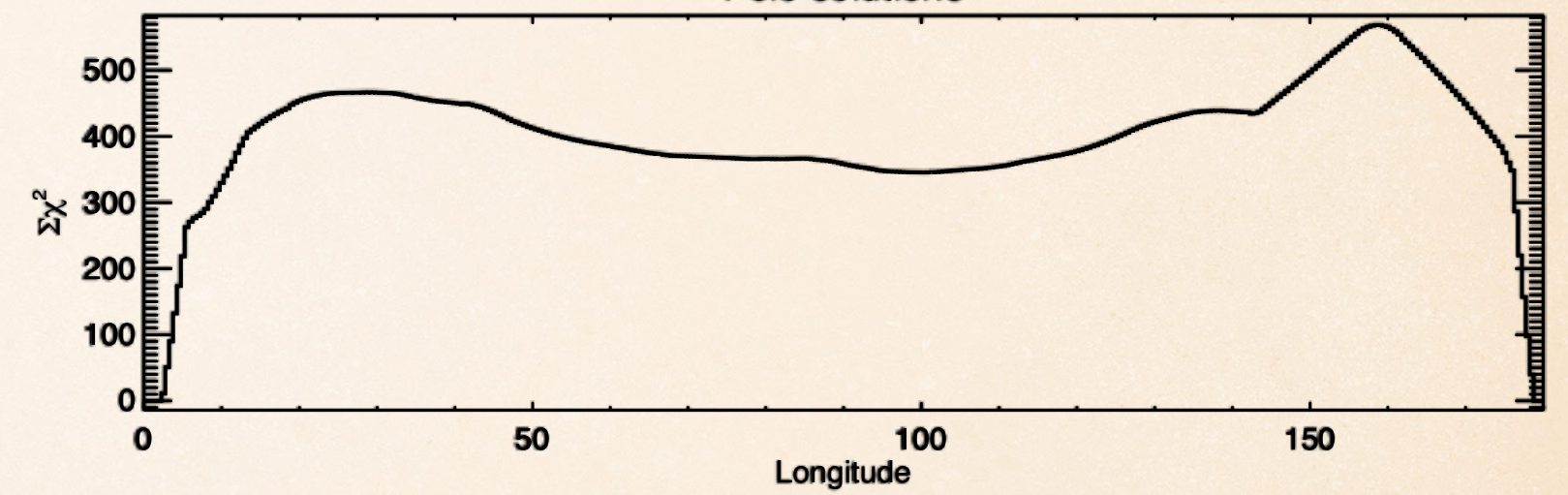
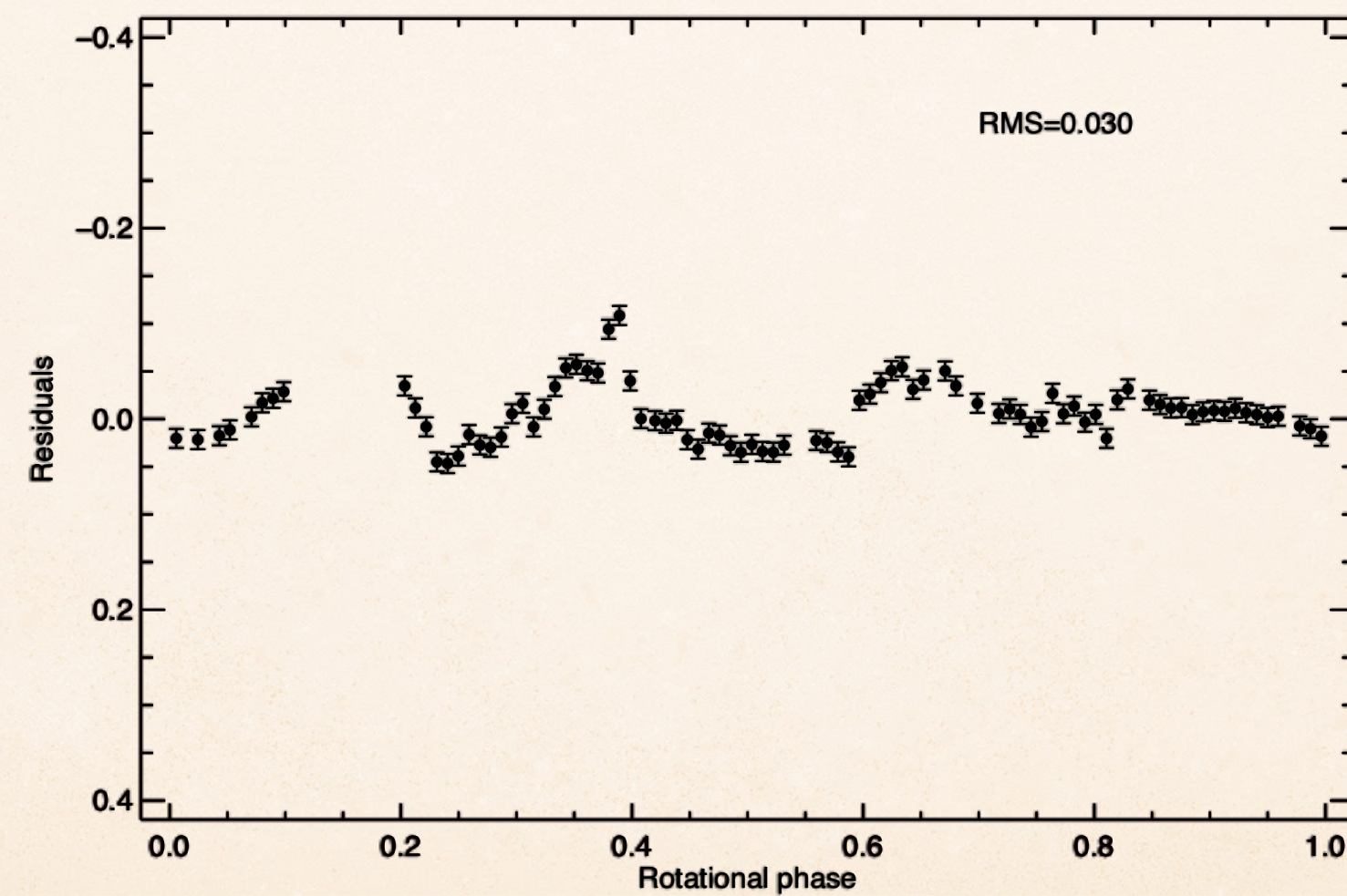
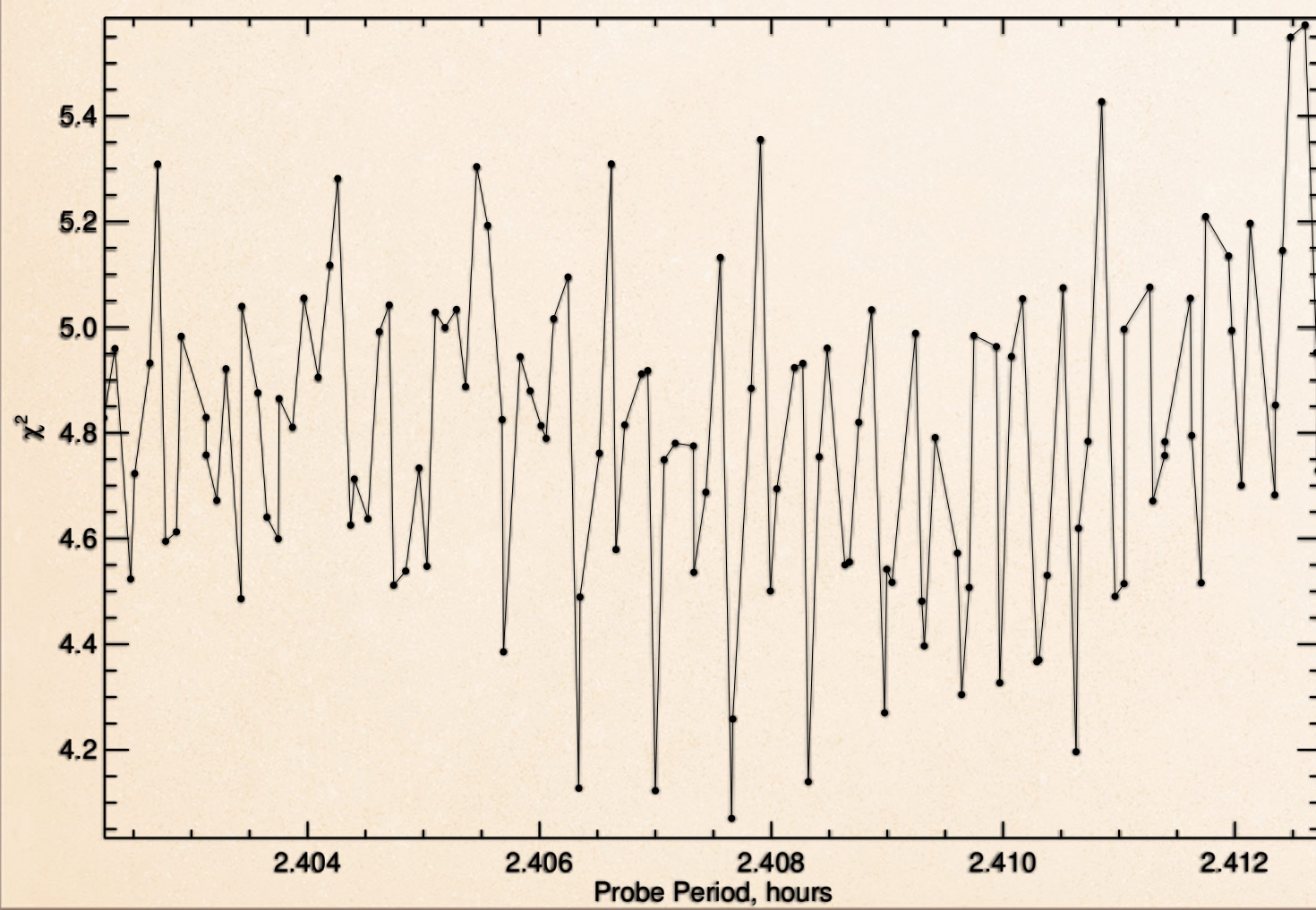
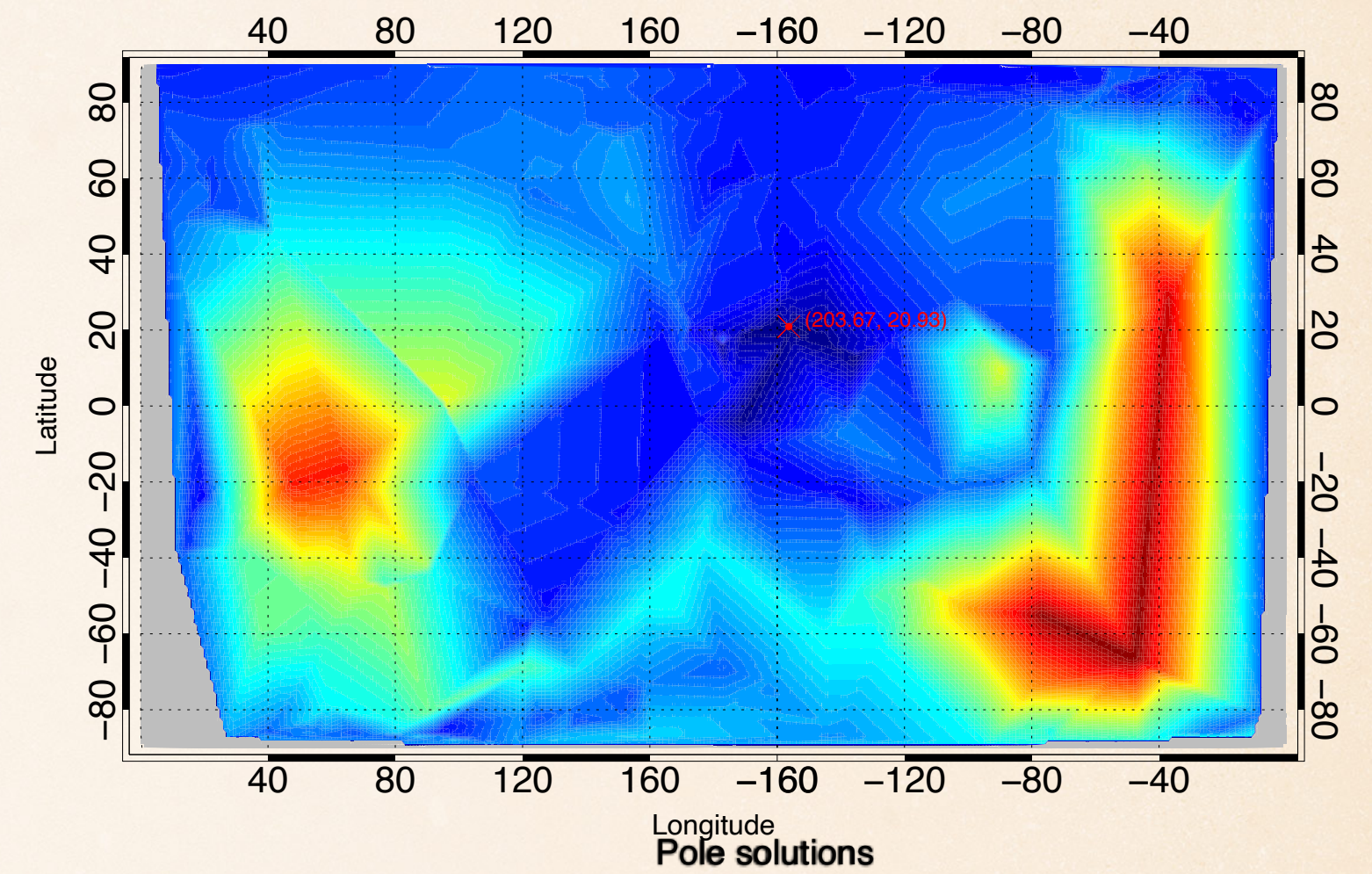
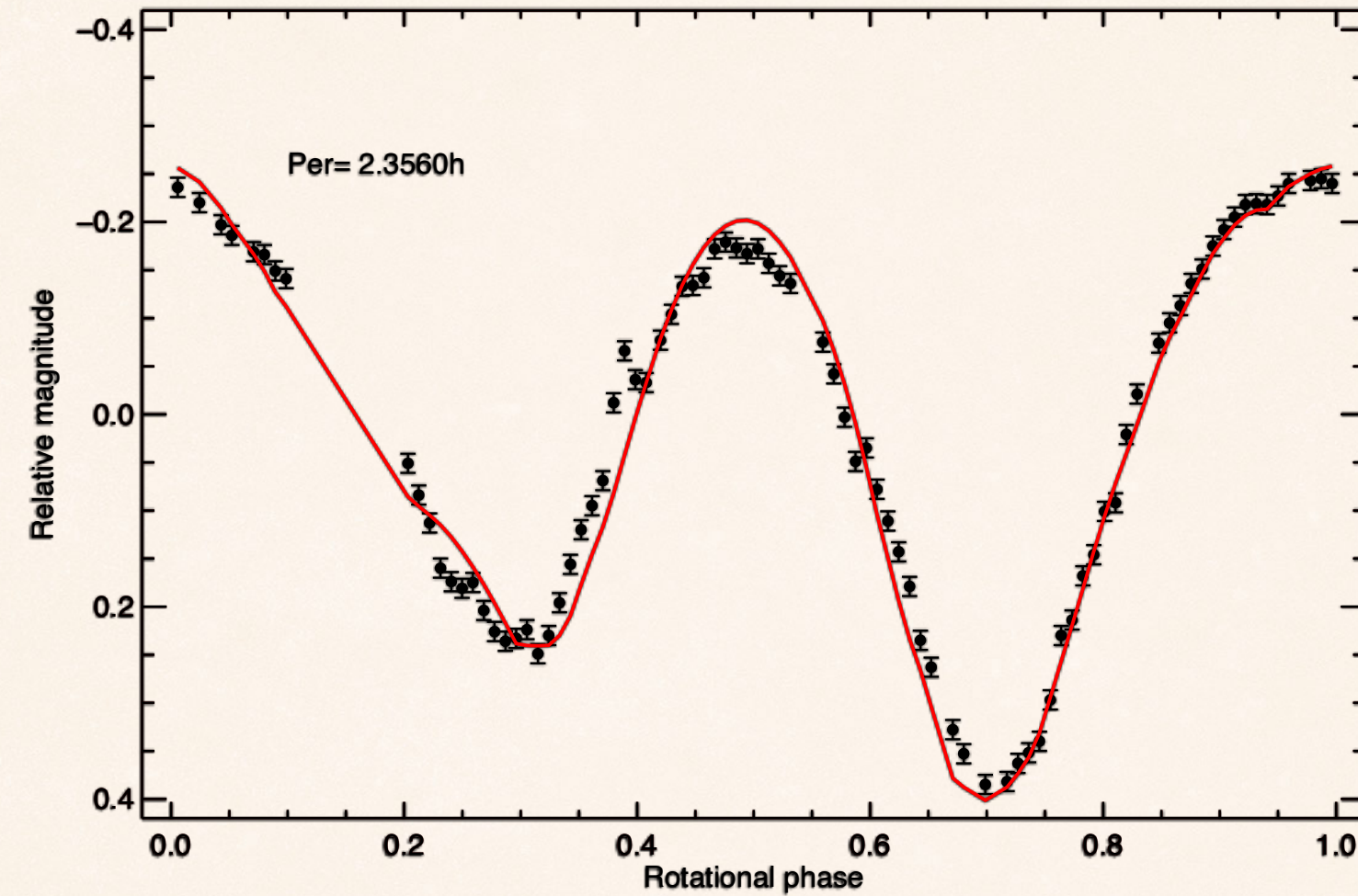
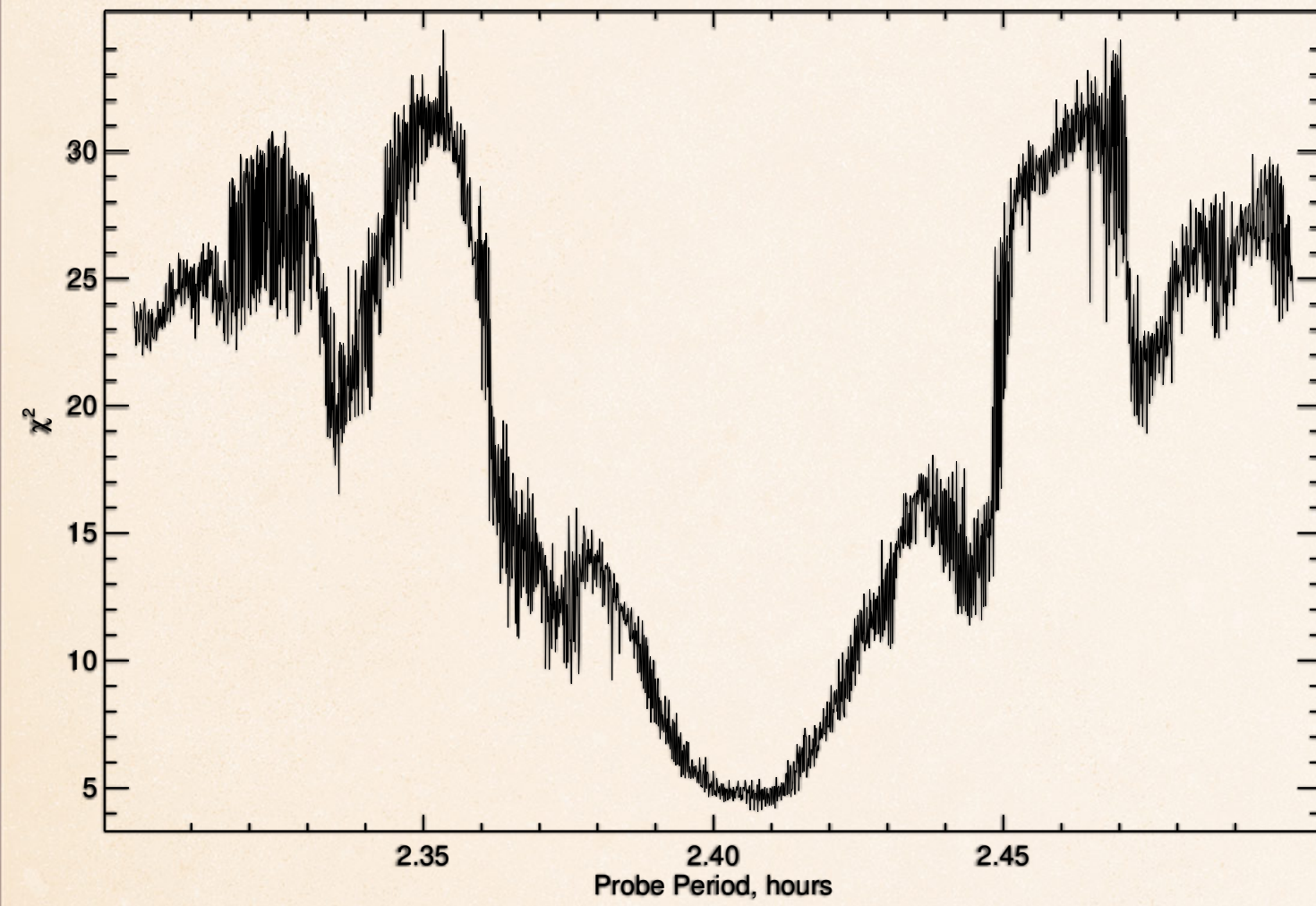
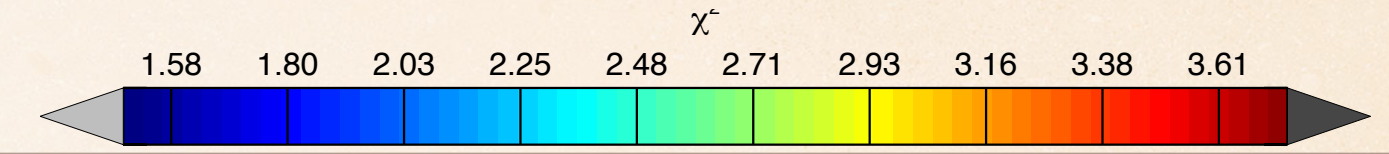
# 2017 SL16 (H=25.8)



# 2016 CA138 (H=23.3)

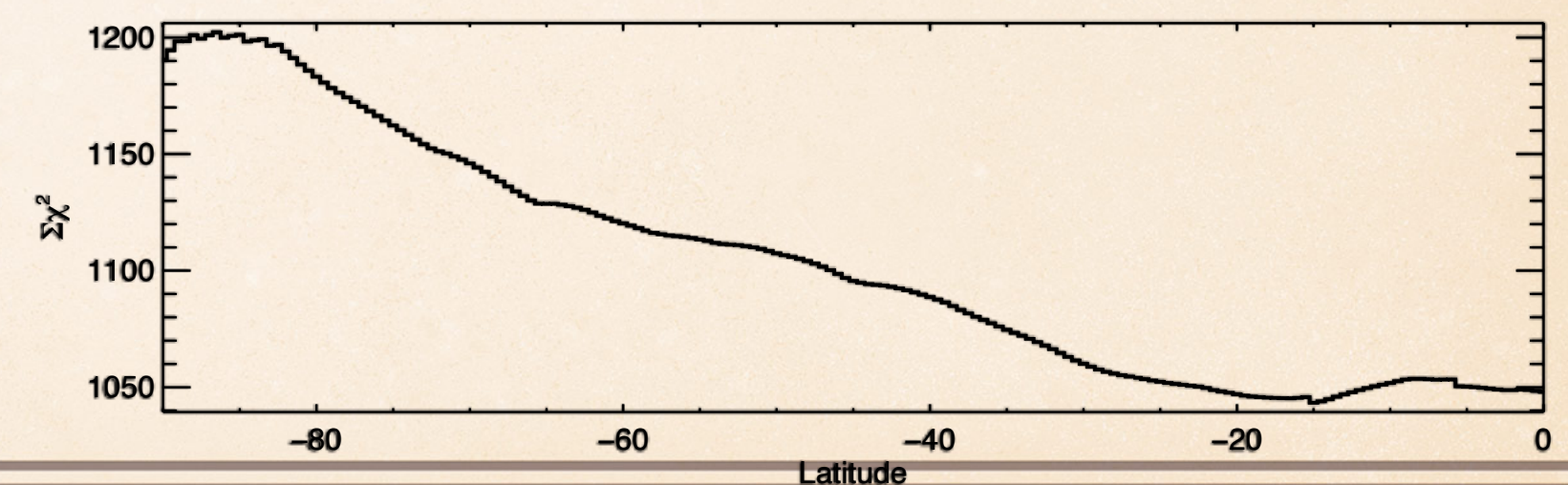
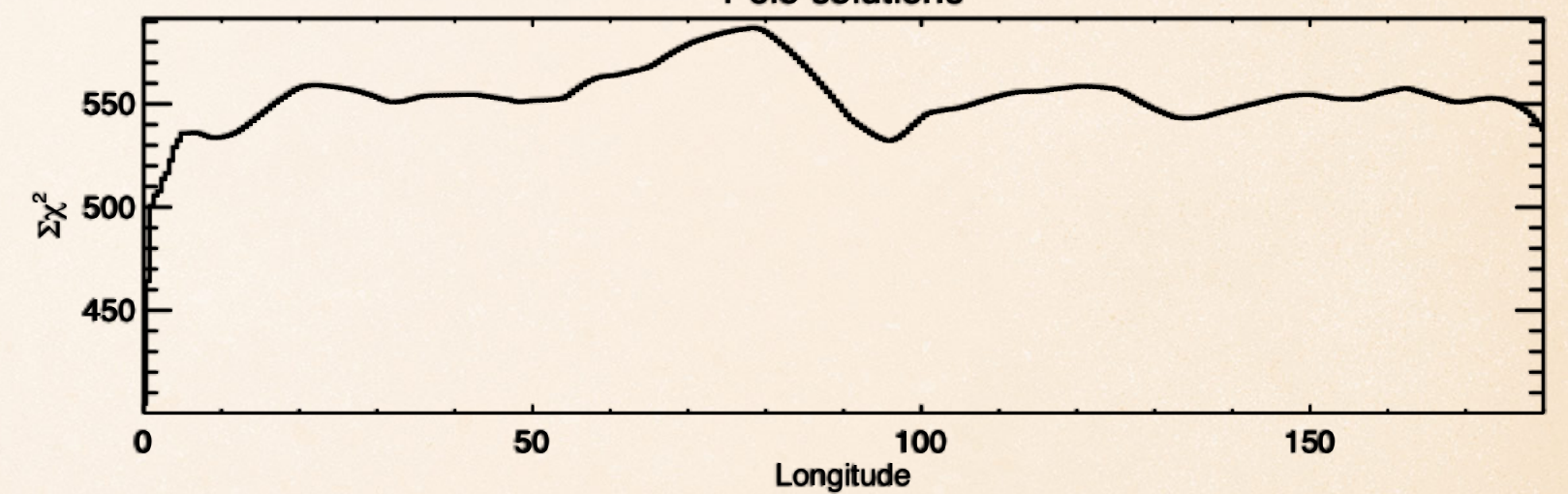
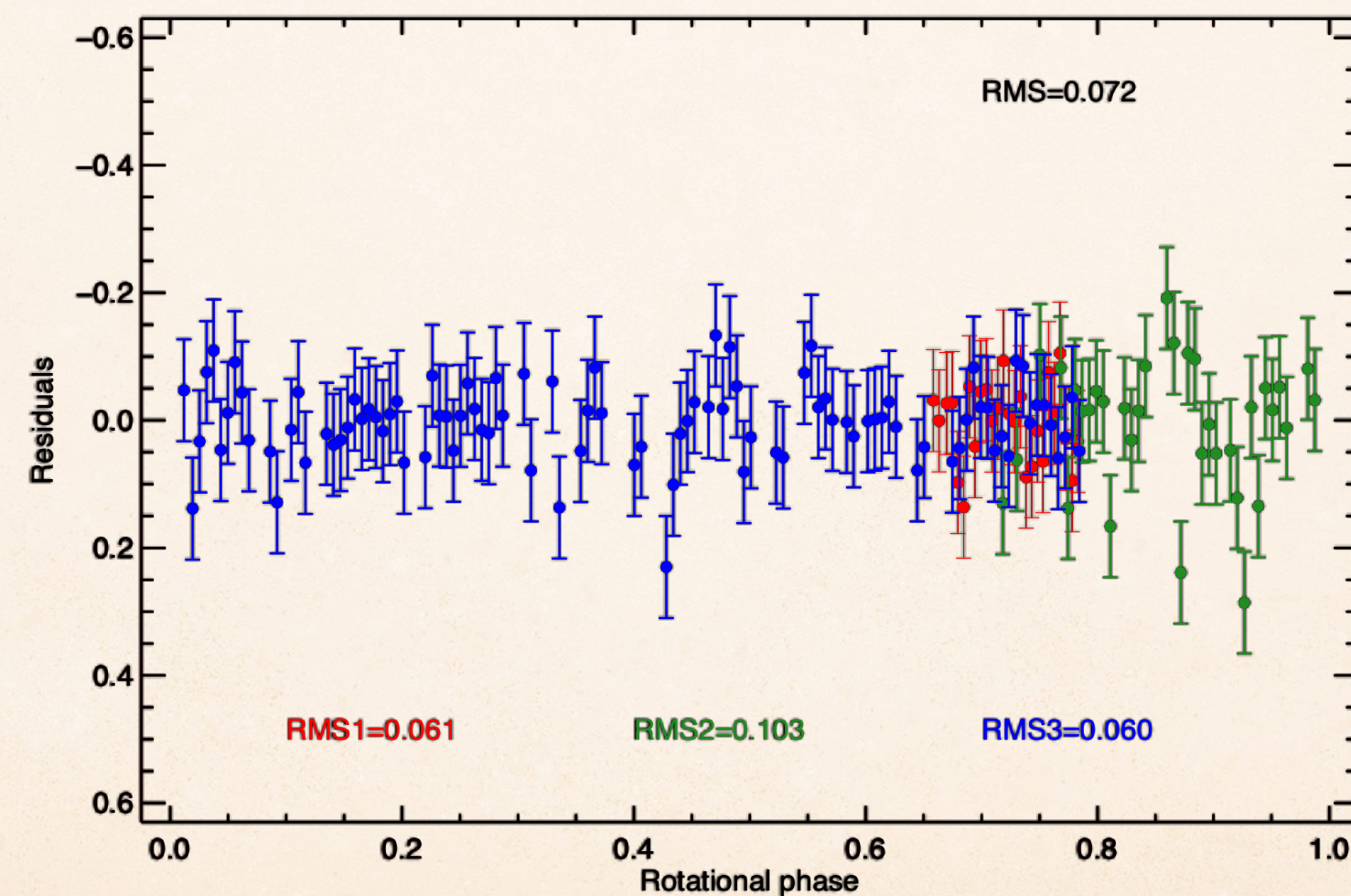
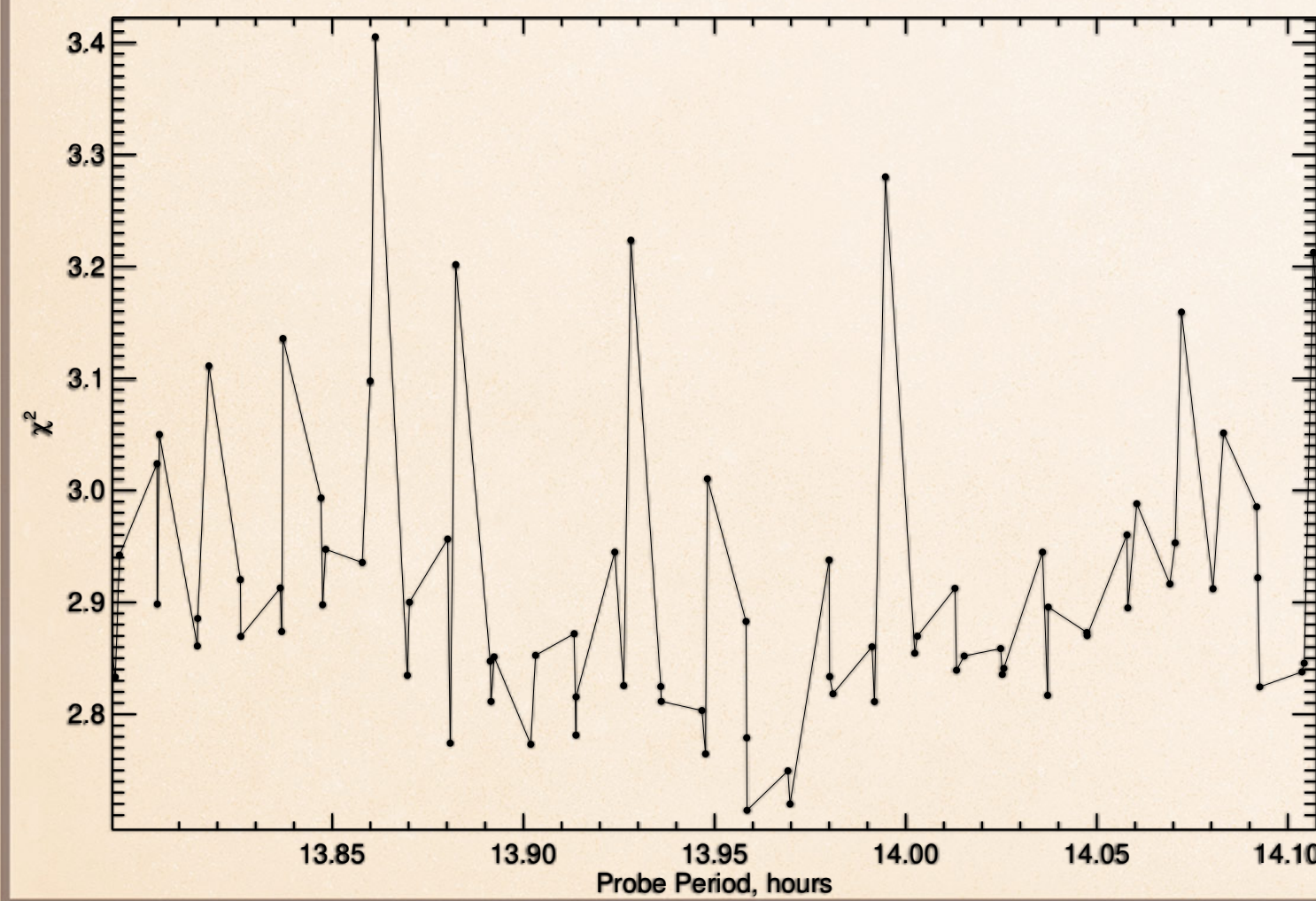
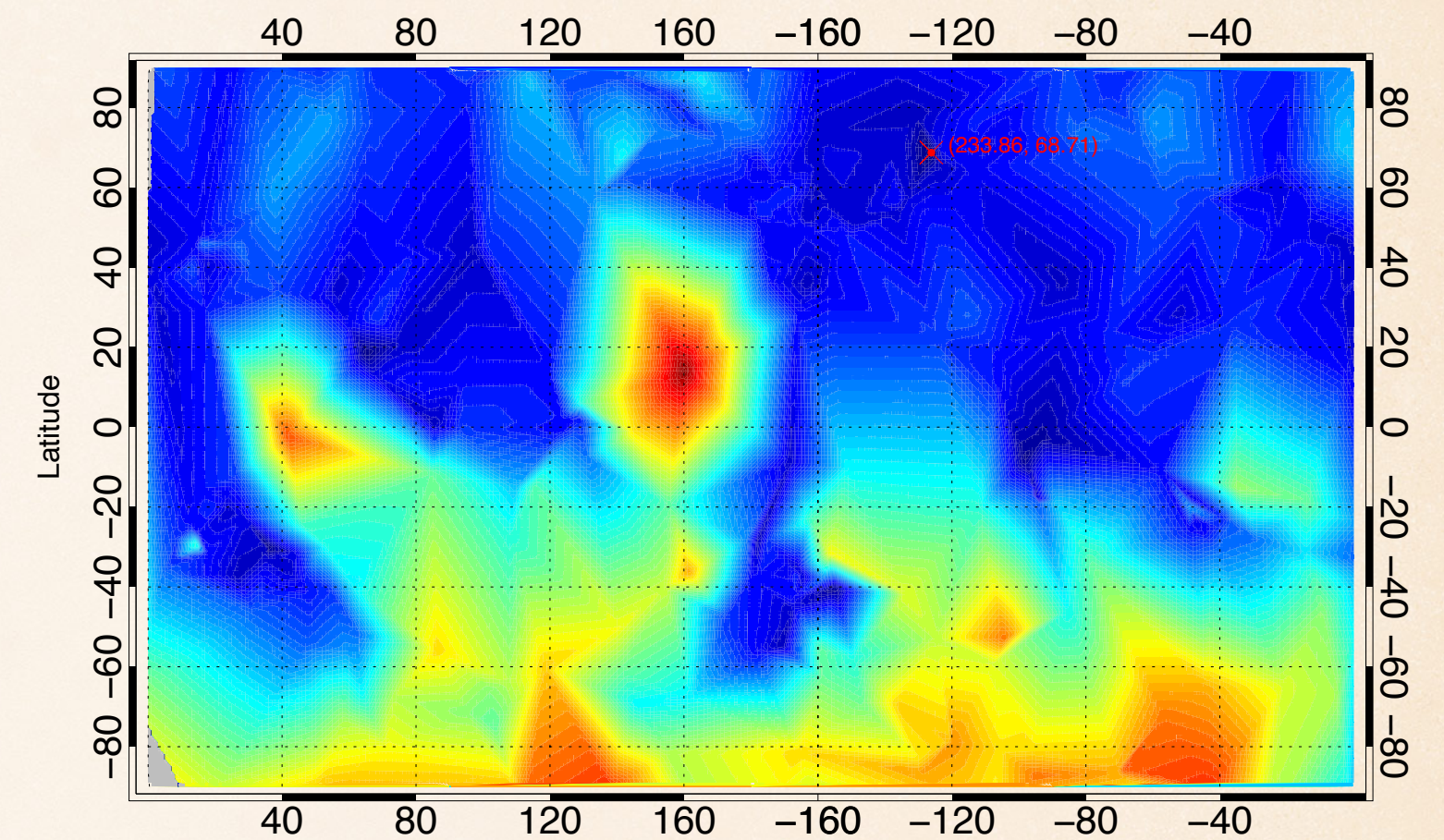
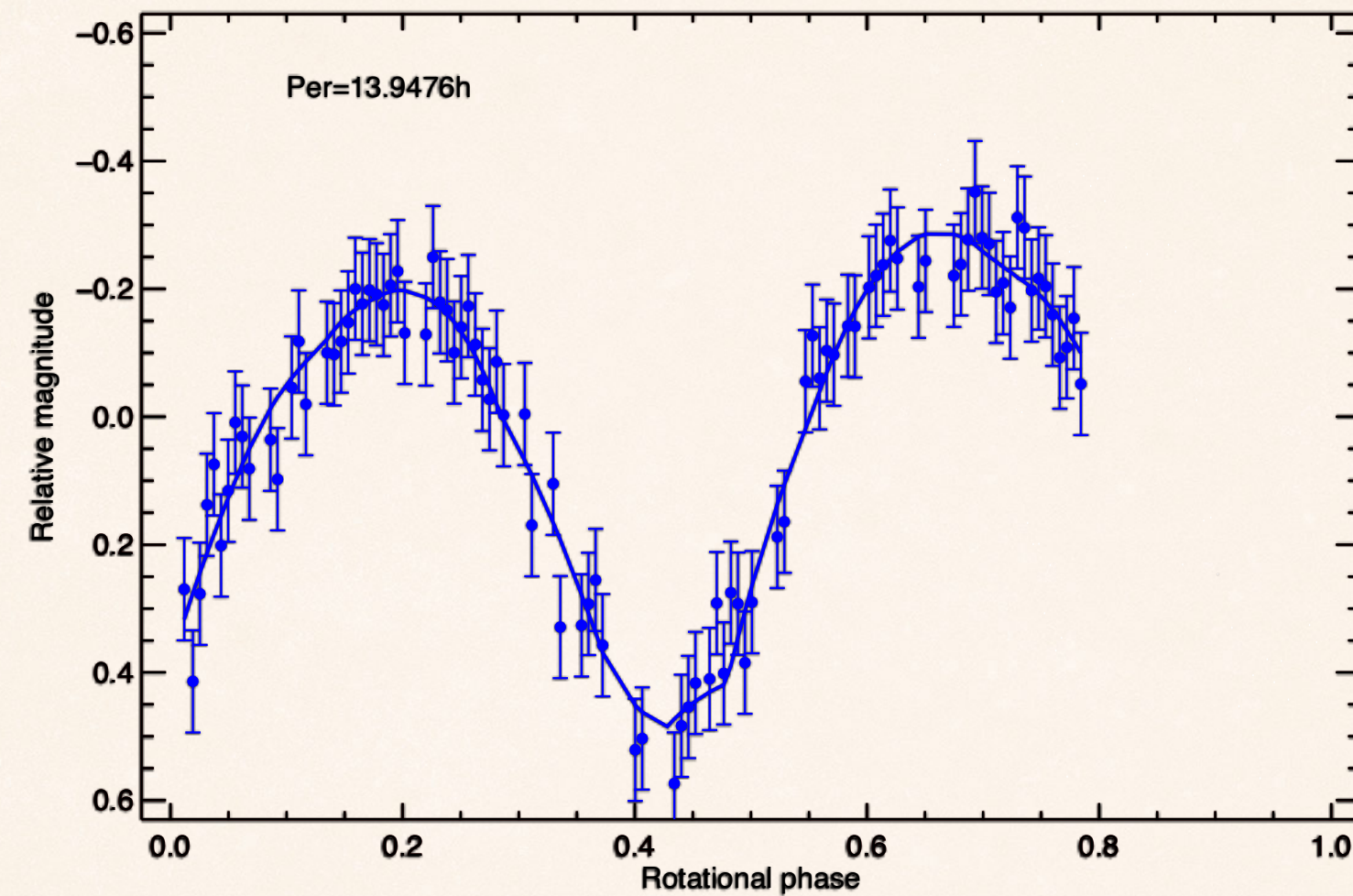
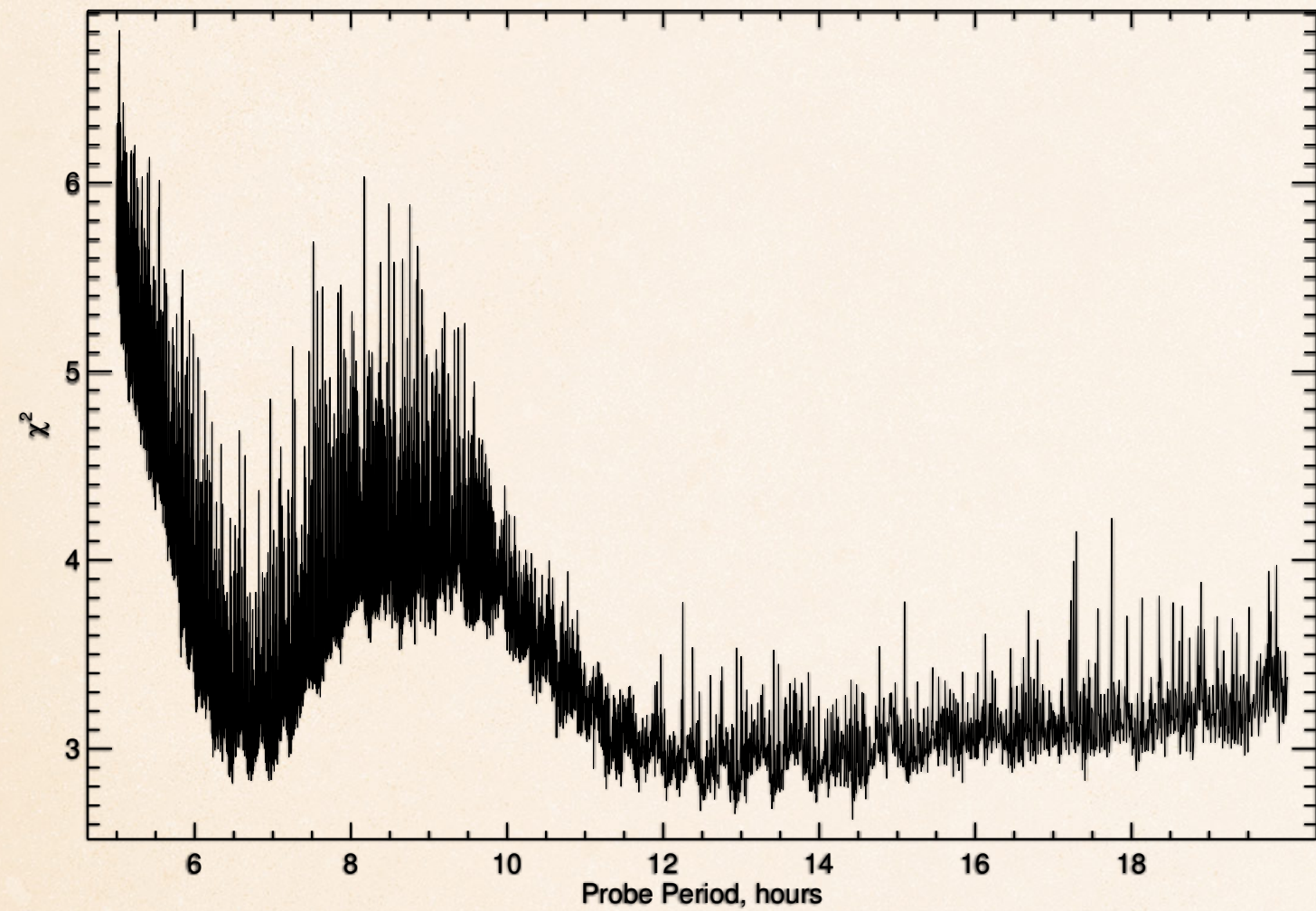
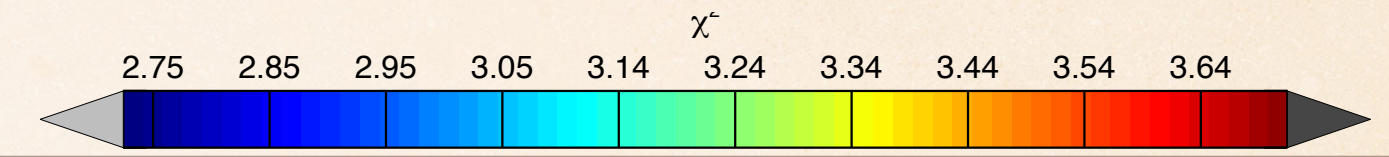


# (418849) 2008 WM64 (H=20.6)



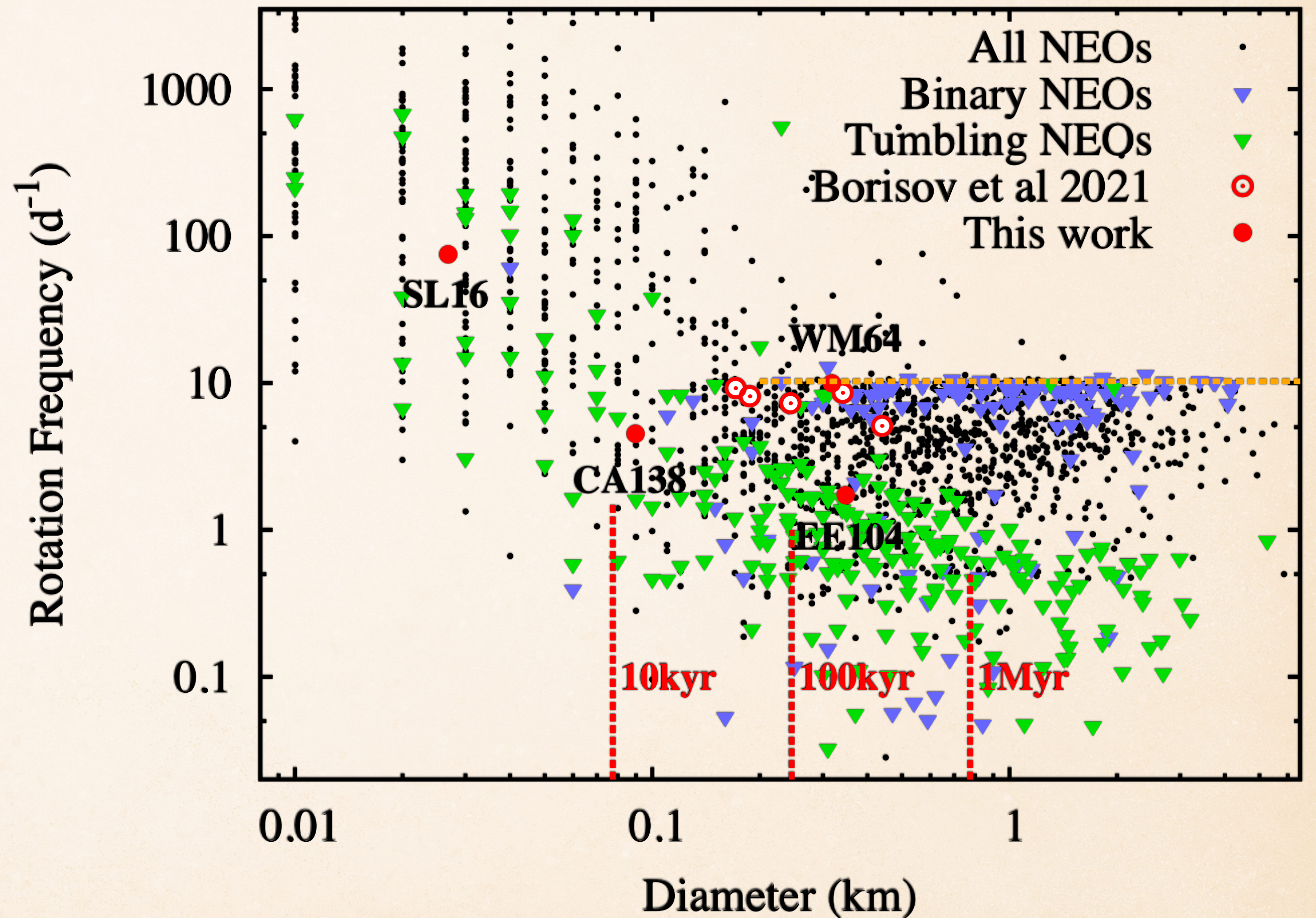


# (138175) 2000 EE104 (H=20.4)



# COMPARISON TO NEAS

Size vs spin rate of co-orbital asteroids in our sample (red points) compared to NEAs entries in the Asteroid Lightcurve Data Base (LCDB Bundle v4.0) as of December 2021, including confirmed binary and tumbling asteroids (blue and green points resp.). The horizontal line corresponds to the critical spin rate  $\omega_{crit}(\rho)$  for  $\rho=2000 \text{ kg.m}^{-3}$ . Overall, co-orbital asteroids in the extended sample appear to have rotation rates similar to NEAs of similar size. Several objects in our sample, including 2008 WM64, cluster near the critical rotation frequency.

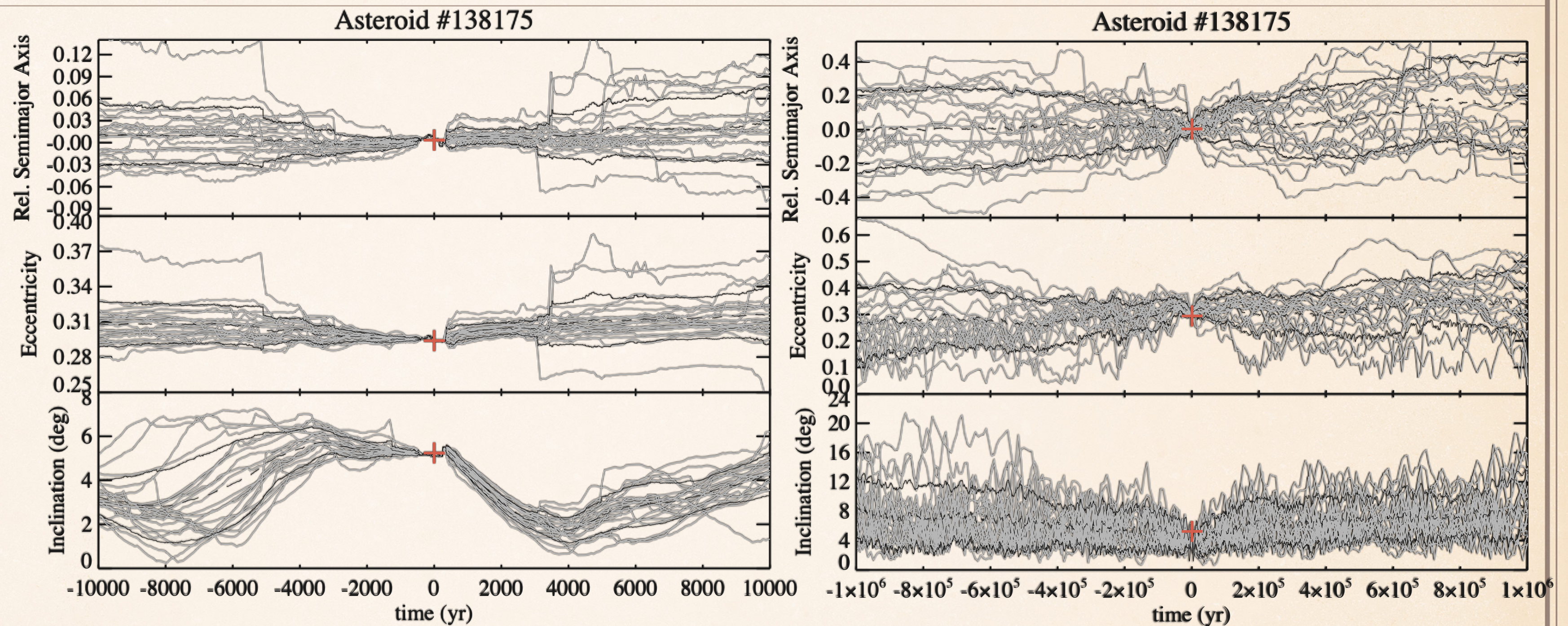


# NUMERICAL SIMULATIONS

- ❖ To investigate the orbit evolution of the asteroids, we used the HYBRID symplectic state propagation scheme available in the MERCURY package
- ❖ Each asteroid was cloned 20 times
- ❖ Two simulation batches were run for the four groups of asteroid clones plus the nominal orbits, one for  $10^4$  yr and the other for  $10^6$  yr, backwards and forwards from the starting epoch. The integration step size in both cases was 4 days, the output step was 10 yr for the  $10^4$  yr runs and  $10^3$  yr for the  $10^6$  yr runs.

# (138175) 2000 EE104 (H=20.4)

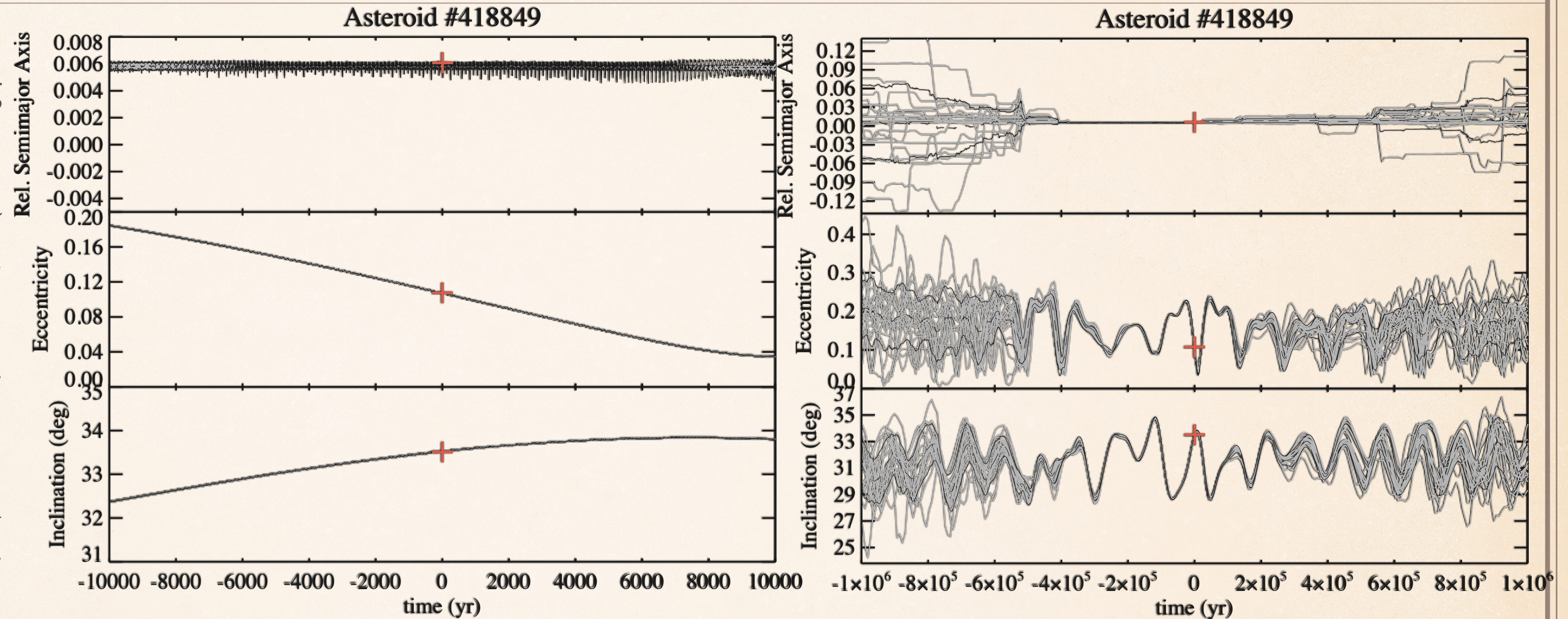
This asteroid has the most unstable orbit of those investigated in this work. This is probably due to its moderate eccentricity and low inclination, allowing frequent and relatively slow encounters with Venus as well as the Earth. None of the clones remains within the Earth's co-orbital region ( $|a-1 \text{ au}| < 0.01 \text{ au}$ ) for more than a few hundred years from the start of the simulations.



Relative semimajor axis  $(a-a_{\text{Earth}})/a_{\text{Earth}}$ , eccentricity  $e$  and inclination  $I$  for the nominal orbit and 20 clones of each asteroid over  $10^4$  yr (left) and  $10^6$  yr (right) from  $t = 0$ .

# (418849) 2008 WM64 (H=20.6)

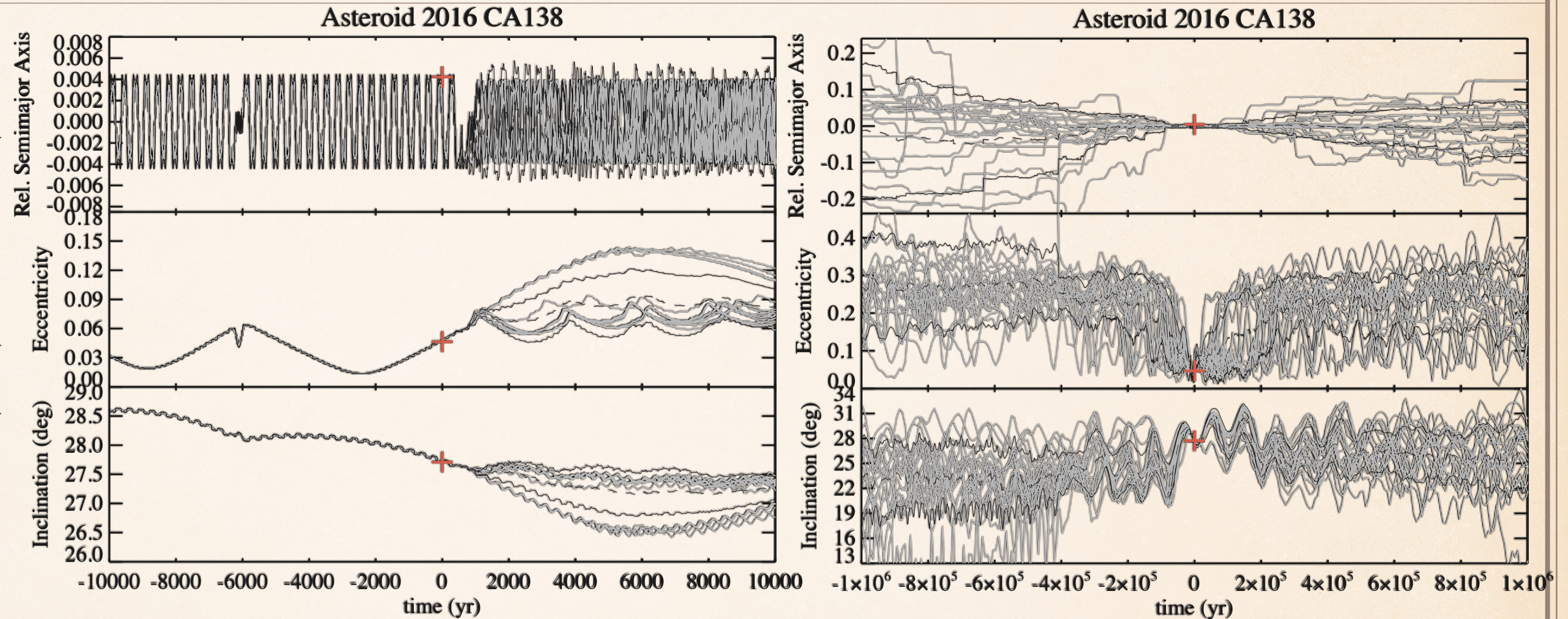
This asteroid is slowly drifting backwards with respect to the Earth in what we refer to as a passing orbit. Our simulations show that all orbits trace identical paths in  $a$ ,  $e$  and  $I$  for at least  $10^4$  yr in the past and in the future. Longer-term, the asteroid has likely been in a passing orbit for the past  $2 \times 10^5$  yr while the future evolution of the orbit is less certain, with the clone semimajor axes beginning to disperse after a few times  $10^4$  yr.



Relative semimajor axis  $(a - a_{\text{Earth}}) / a_{\text{Earth}}$ , eccentricity  $e$  and inclination  $I$  for the nominal orbit and 20 clones of each asteroid over  $10^4$  yr (left) and  $10^6$  yr (right) from  $t = 0$ .

# 2016 CA138 (H=23.3)

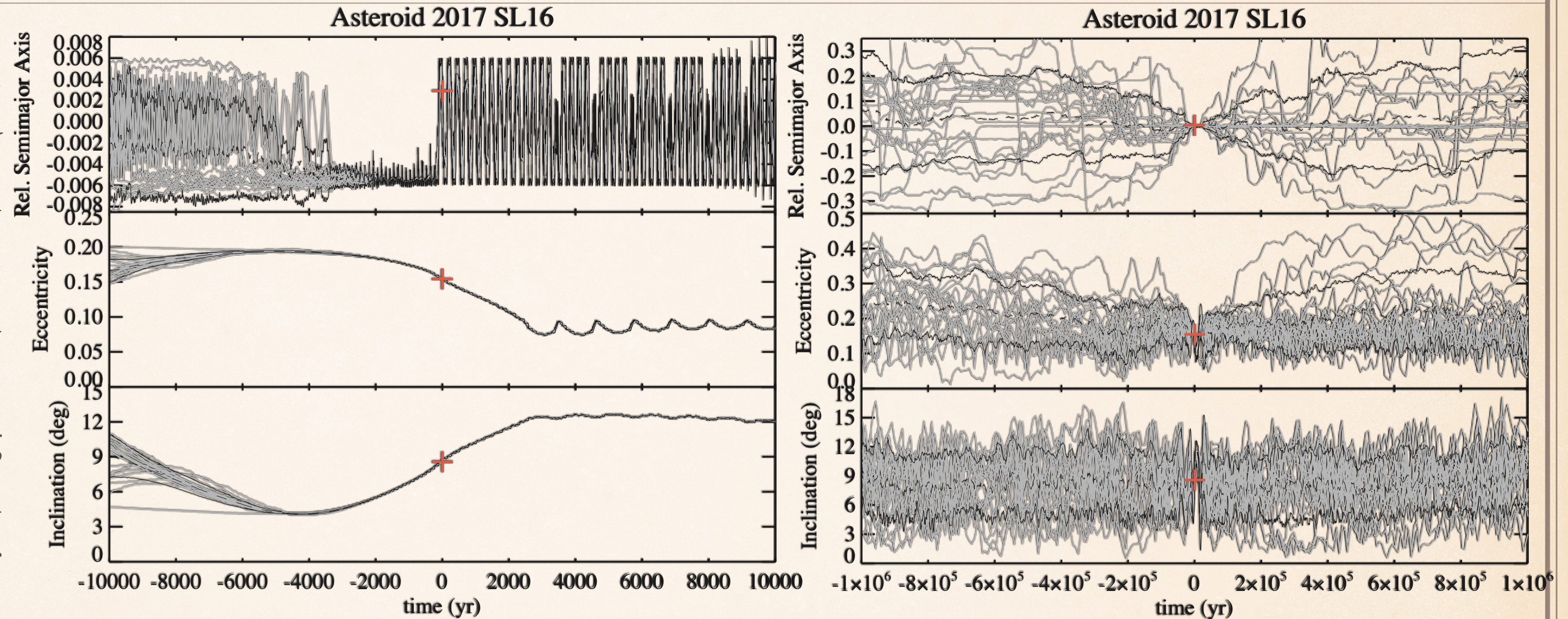
This asteroid is currently in an Earth horseshoe orbit, qualifying therefore as the 13th Earth horseshoe. In our 1 Myr runs, we find that confinement of the asteroid's orbit within the Earth's co-orbital region persists for several times  $10^4$  yr in the past and in the future.



Relative semimajor axis  $(a-a_{\text{Earth}})/a_{\text{Earth}}$ , eccentricity  $e$  and inclination  $I$  for the nominal orbit and 20 clones of each asteroid over  $10^4$  yr (left) and  $10^6$  yr (right) from  $t = 0$ .

# 2017 SL16 (H=25.8)

The orbital evolution of this asteroid was recently investigated by Kaplan and Cengiz (2020). Those authors showed that SL16 is currently in an QS-HS asymmetric horseshoe configuration, having transitioned into this state from a passing orbit  $\sim 100$  yr ago. Our simulations of the asteroid's orbital evolution up to  $10^4$  yr from the present are in very good agreement with Kaplan and Cengiz.



Relative semimajor axis  $(a-a_{\text{Earth}})/a_{\text{Earth}}$ , eccentricity  $e$  and inclination  $I$  for the nominal orbit and 20 clones of each asteroid over  $10^4$  yr (left) and  $10^6$  yr (right) from  $t = 0$ .

## OVERALL DYNAMICAL PROPERTIES AND RELATION TO ROTATIONAL STATE

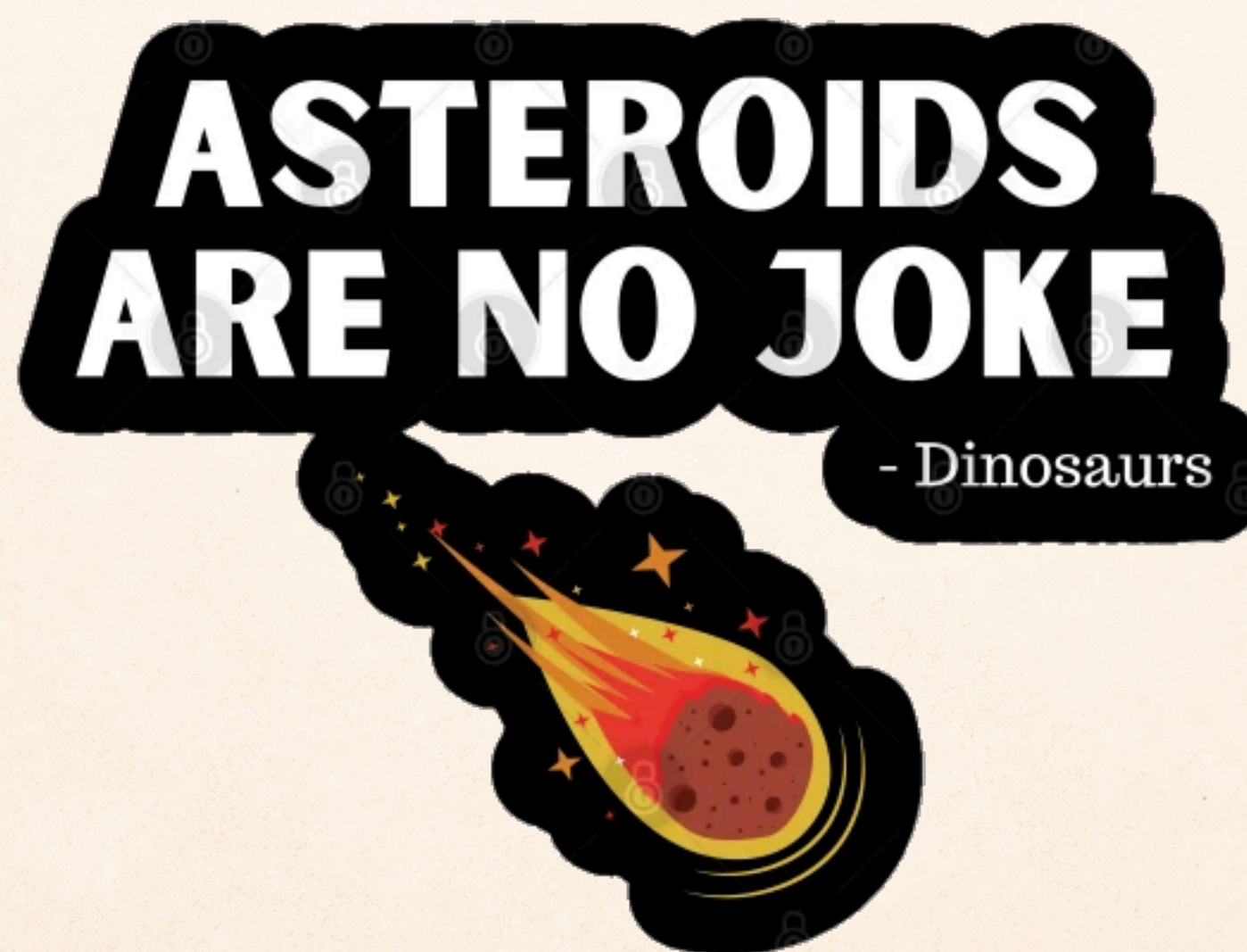
- ❖ Our results show that the co-orbital resonance is not affecting the orbit stability, but the orbit itself is responsible for that and mainly its eccentricity ( $e$ ) and inclination ( $I$ ). Orbits with low  $e$  and high  $I$  are the most stable because firstly high-incline orbit avoids frequent close encounters with planets and secondly orbits with high  $e$  may approach Venus as well as the Earth.
- ❖ We cannot make a definitive conclusion if the orbit stability and rotational state of the asteroids are related, so we need further investigations and observations to increase our sample in order to obtain more statistically significant results.



THANKS FOR YOUR ATTENTION!

THANKS FOR YOUR ATTENTION!

BUT KEEP IN MIND





# YARKOVSKY

- ❖ A question to be asked here is whether including the size-dependent Yarkovsky drag force in our dynamical model might change the outcome in a significant way.
- ❖ Fenucci and Novaković (2020) investigated this question for the Earth quasi-satellite (469219) Kamo'oalewa, an object comparable in both size and orbit to the smallest object in our sample, 2017 SL16. Though Yarkovsky does change the orbital evolution of Kamo'oalewa over millions of yr and its residence time as an Earth co-orbital, actual differences from the gravity-only case were quite small and the overall effect on the evolution of the orbit was not significant. For this reason, and to minimise the computational overhead of our runs, we decided not to include the Yarkovsky effect in our simulations.

# 3D SHAPE MODELS

